TECHNICAL REPORT ARBRL-TR-02458

TRANSONIC SHOCK-TURBULENT BOUNDARY LAYER INTERACTIONS ON SPINNING AXISYMMETRIC BODIES AT ZERO ANGLE OF ATTACK

George R. Inger

January 1983

US ARMY ARMAMENT RESEARCH AND DEVELOPMENT COMMAND
BALLISTIC RESEARCH LABORATORY
ABERDEEN PROVING GROUND, MARYLAND

Destroy this report when it is no longer needed.
Do not return it to the originator.

Secondary distribution of this report is prohibited.

Additional copies of this report may be obtained from the National Technical Information Service, U. S. Department of Commerce, Springfield, Virginia 22161.

The findings in this report are not to be construed as an official Department of the Army position, unless so designated by other authorized documents.

The use of trade names or manufacturers' names in this report does not constitute indorsement of any commercial product.

UNCLASSIFIED

SECURITY CLASSIFICATION OF THIS PAGE *(When Data Entered)*

REPORT DOCUMENTATION PAGE		READ INSTRUCTIONS BEFORE COMPLETING FORM
1. REPORT NUMBER Technical Report ARBRL-TR-02458	2. GOVT ACCESSION NO.	3. RECIPIENT'S CATALOG NUMBER
4. TITLE *(and Subtitle)* TRANSONIC SHOCK-TURBULENT BOUNDARY LAYER INTERACTIONS ON SPINNING AXISYMMETRIC BODIES AT ZERO ANGLE OF ATTACK		5. TYPE OF REPORT & PERIOD COVERED Final 6. PERFORMING ORG. REPORT NUMBER
7. AUTHOR(s) George R. Inger		8. CONTRACT OR GRANT NUMBER(s)
9. PERFORMING ORGANIZATION NAME AND ADDRESS U.S. Army Ballistic Research Laboratory (ATTN: DRDAR-BLL) Aberdeen Proving Ground, Maryland 21005		10. PROGRAM ELEMENT, PROJECT, TASK AREA & WORK UNIT NUMBERS RDT&E 1L161102AH43
11. CONTROLLING OFFICE NAME AND ADDRESS US Army Armament Research & Development Command US Army Ballistic Research Laboratory (DRDAR-BL) Aberdeen Proving Ground, Maryland 21005		12. REPORT DATE January 1983 13. NUMBER OF PAGES 75
14. MONITORING AGENCY NAME & ADDRESS*(if different from Controlling Office)*		15. SECURITY CLASS. *(of this report)* Unclassified 15a. DECLASSIFICATION/DOWNGRADING SCHEDULE

16. DISTRIBUTION STATEMENT *(of this Report)*

Approved for public release, distribution unlimited.

17. DISTRIBUTION STATEMENT *(of the abstract entered in Block 20, if different from Report)*

18. SUPPLEMENTARY NOTES

19. KEY WORDS *(Continue on reverse side if necessary and identify by block number)*

Transonic Flow
Turbulent Viscous Flow
Shock-Boundary Layer Interaction

20. ABSTRACT *(Continue on reverse side if necessary and identify by block number)*

This report presents a detailed triple-deck theory of the transonic shock - nonseparating turbulent boundary layer interaction zones on spinning axisymmetric bodies at zero angle of attack. The theory allows a general non-equilibrium turbulent boundary layer history upstream of the interaction. We further describe the application of this theory as a local interactive module imbedded in a global composite viscous-inviscid transonic flow field prediction method which can handle two or more such interaction zones. Detailed

DD FORM 1 JAN 73 1473 EDITION OF 1 NOV 65 IS OBSOLETE

UNCLASSIFIED

SECURITY CLASSIFICATION OF THIS PAGE *(When Data Entered)*

comparisons with both experimental data and thin-layer Navier-Stokes code predictions are presented to verify the accuracy and reliability of the composite method solutions for pressure, displacement thickness, velocity profiles, shape factor and skin friction distributions along the body over a wide range of Mach/Reynolds number conditions.

TABLE OF CONTENTS

TABLE OF CONTENTS (continued)

LIST OF ILLUSTRATIONS

LIST OF ILLUSTRATIONS (continued)

I. INTRODUCTION

The aerodynamic characteristics of standard artillery shell from subsonic to supersonic speeds is of major concern in the design of new shell or modifications to existing ones. The possibility that a given shape may have to operate throughout a range of Mach numbers requires a detailed understanding of the flow fields associated with each range. Modern computational techniques are now being applied to projectile shapes and the ability to compute the aerodynamics of shell for a wide range of Mach numbers and Reynolds numbers is becoming a reality. Significant accomplishments have been made in the supersonic regime[1]: static and Magnus force coefficients have been computed for standard projectile configurations and experimental data is generally available which shows good comparisons with theory. Transonic flow, however, presents a new complexity for computational analysis. The formation of shock waves, imbedded in the flow field near surface discontinuities, produces a severe change of the aerodynamic coefficients such as drag and pitching moments. For example, the drag of a projectile shape has been found to change by as much as 100% through a Mach number range of .95 to .97. A change of this magnitude in the aerodynamics makes it essential to understand and compute the features of the flow field which contribute to this effect.

The transonic flow field around a projectile presents a difficult and interesting problem; the general features of the flow pattern are illustrated in Figure 1, which is a shadowgraph of a typical projectile flying at $M_\infty = .946$. The two surface shape discontinuities create local expansion zones terminated by shock waves through which the boundary layer must pass, thereby creating a pair of viscous-inviscid interaction regions. The existance of these regions together with the cylindrical geometry of projectiles clearly produces a composite inviscid-viscous flow field problem not encountered in the design of normal winged aircraft.

Although some comprehensive transonic flow field investigations have been made on transonic wings[2,3], comparable efforts have not been made for bodies of revolution particularly if spinning. Existing studies have been primarily concerned with surface pressure distributions and inviscid flow predictions with only sparse consideration of the boundary layer and transonic viscous-

---

1. *Sturek, W. B., et al., "Computations of Magnus Effects for a Yawed, Spinning Body of Revolution;" AIAA Journal, Vol. 16, No. 7, July 1978, pp. 687-692.*

2. *Rose, W. C., and Segniner, A., "Calculation of Transonic Flow Over Supercritical Airfoil Sections," AIAA Journal 15, August 1978, pp. 514-519.*

3. *Sobieczky, M., and Stanewsky, E., "The Design of Transonic Airfoils Under Consideration of Shock Wave-Boundary Layer Interaction," 10 ICAS Congress Paper, October 1976 (see also E. Stanewsky and H. Zimmer, Zeit. fur Flugwissenschaften 23, Heft 7/8, 1975).*

inviscid interaction effects throughout the flow field[4,5]. Consequently, a comprehensive fundamental investigation of the combined inviscid-viscous flow field problem on transonic artillery projectiles was undertaken at BRL with the objective of developing an appropriate composite theoretical treatment including the shock-boundary layer interaction effects, together with validating comparisons with experiment. The present report describes the results of this study for the case of projectile flight at zero angle of attack, with emphasis on a description of the theoretical work involved in treating the interaction problem. Since the approach taken has been to extend Inger's theory[6] of non-separating transonic shock-turbulent boundary layer interactions to spinning bodies of revolution, we first highlight the 2-D version of this theory in Section 2. The desired extension of the theory is then given in Section 3, followed in Section 4 by a description of how the local interaction theory is combined with inviscid transonic and turbulent boundary layer prediction methods to form a composite global inviscid-viscous flow field prediction code for the entire body. Finally, Section 5 presents comparisons of this theory with both experimental data and numerical solutions based on the thin-layer Navier-Stokes equations.

II. OUTLINE OF THE LOCAL INTERACTION THEORY FOR TWO-DIMENSIONAL FLOWS

A. Rationale of Non-Asymptotic Triple Deck Approach

It is well-known[7] that when separation occurs, the disturbance flow pattern associated with a nearly-normal shock-boundary layer interaction is a very complicated one involving a bifurcated shock pattern, whereas the unseparated case pertaining to turbulent boundary layers up to roughly $M_1 \approx 1.3$ has instead a much simpler type of interaction pattern which is more amenable to analytical treatment (see Figure 2). With some judicious simplifications, it is possible to construct a fundamentally-based approximate theory of the

---

4. *Wu, J. C., Moulden, T.H., and Uchiyama, N., "Aerodynamic Performance of Missile Configurations at Transonic Speeds Including the Effects of a Jet Plume," U.S. Army Missile Command Technical Report RD-76-23, Redstone Arsenal, Alabama, March 1976.*

5. *Reklis, R. P., Sturek, W. B., and Bailey, F. R., "Computation of Transonic Flow Past Projectiles at Angle of Attack," AIAA 11th Fluid and Plasma Dynamics Conference, AIAA Paper No. 78-1182, July 1978.*

6. *Inger, G. R., "Upstream Influence and Skin Friction in Non-Separating Shock Turbulent Boundary Layer Interactions," AIAA Paper 80-1411, Snowmass, Colorado, July 1980.*

7. *Ackeret, J., Feldman, F., and Rott, N., "Investigations of Compression Shocks and Boundary Layers in Gases Moving at High Speed," NACA TM-1113, January 1947.*

problem, as documented in detail in Reference 6. For purposes of orientation and completeness, a brief outline of this theory will be given here.

We consider small disturbances of an arbitrary incoming turbulent boundary layer due to a weak external shock and examine the detailed perturbation field within the layer. We purposely employ a non-asymptotic triple-deck flow model patterned in some ways after Lighthill's approach[8] because of its essential soundness and adaptability to further improvement, because of its similarity to related types of multiple-deck approaches that have proven highly successful in treating turbulent boundary layer response to strong known adverse pressure gradients[9], and because of the large body of turbulent boundary layer interaction data that supports the predicted results in a variety of specific problems[6]. At high Reynolds numbers it has been established[10,11,12] that the local interaction disturbance field in the neighborhood of the impinging shock organizes itself into three basic layered-regions or "decks" (Figure 3): 1) an outer region of potential inviscid flow above the boundary layer, which contains the incident shock and interactive wave systems; 2) an intermediate deck of frozen shear stress-rotational inviscid disturbance flow occupying the outer 90% or more of the incoming boundary layer thickness; 3) an inner shear-disturbance sublayer adjacent to the wall which accounts for the interactive skin friction perturbations (and hence any possible incipient separation) plus most of the upstream influence of the interaction. The "forcing function" of the problem here is thus impressed by the outer deck upon the boundary layer; the middle deck couples this to the response of the inner deck but in so doing can itself modify the disturbance field to some extent, while the slow viscous flow in the thin inner deck reacts very strongly to the pressure gradient disturbances imposed by these overlying decks. This triple

---

8. *Lighthill, M. J., "On Boundary Layers and Upstream Influence; II. Supersonic Flow Without Separation,"* Proc. Royal Soc. A 217, *1953, pp. 478-507.*

9. *Stratford, B. S., "The Prediction of Separation of the Turbulent Boundary Layer,"* Jour. Fluid Mech. 5, *pp. 1-16, 1959.*

10. *Inger, G. R., and Mason, W. H., "Analytical Theory of Transonic Normal Shock-Boundary Layer Interaction,"* AIAA Paper 75-831, *June 1975 (abbreviated version published in* AIAA Jour. 14, *pp. 1266-72, September 1976).*

11. *Melnik, R. E., and Grossman, B., "Analysis of the Interaction of a Weak Normal Shock Wave with a Turbulent Boundary Layer,"* AIAA Paper 74-598, *June 1974.*

12. *Adamson, T. C., and Feo, A., "Interaction Between a Shock Wave and a Turbulent Layer in Transonic Flow,"* SIAM Journal. Appl. Math 29, *July 1975, pp. 121-144.*

deck structure also has been employed in the theoretical studies of Gadd[13], Lighthill[8], Stratford[9], Honda[14] and others, and has been verified by a large body of experimental evidence and recent numerical studies with the full Navier-Stokes equations[15]. The essential correctness of this model is further supported by its success in related boundary layer perturbation problems involving viscous-inviscid interactions, turbulent boundary layer response to sudden changes in surface roughness or pressure gradient, and flow past various kinds of surface distortions including skin friction measuring devices (see Reference 6).

While there is general agreement about the validity of the triple deck approach over a wide range of Reynolds number and the well-known qualitative differences in interactive response between laminar and turbulent flow (e.g., the much smaller upstream influence and larger separation-resistance of the later), questions have been raised concerning (a) the relative interactive importance of the inner shear-disturbance deck and (b) the accuracy of deliberately using a non-asymptotic treatment of the details within the boundary layer. Regarding the first, we note that while asymptotic ($Re_\ell \to \infty$) theory predicts an exponentially-small thickness and displacement effect contribution of the inner deck[9,10], this is not apparently true at ordinary Reynolds numbers, where many analytic and experimental studies have firmly established that this deck, although indeed very thin, still contributes significantly to the overlying interaction and its displacement thickness growth[6]. Bolstered by these facts, plus the unanimous conclusion reached in the detailed reviews by Green[16], Rose, Murphy and Watson[17], and Hankey and Holden[18] that the viscous sublayer is an important component of turbulent interaction problems, we take the point of view here that the inner deck is in fact significant at

---

13. *Gadd, G. E., "Interactions Between Wholly Laminar or Wholly Turbulent Boundary Layers and Shock Wave Strong Enough to Cause Separation," Jour. of the Aeronaut. Sci. 20, November 1953, p. 729.*

14. *Honda, M., "A Theoretical Investigation of the Interaction Between Shock Waves and Boundary Layers," Jour. Aero/Space Sci. 25, November 1958, pp. 667-677.*

15. *Hankey, W., and Shang, J., "Numerical Solution of the Navier-Stokes Equations for Supersonic Turbulent Flow over a Compression Ramp," AIAA Paper 75-3, Pasadena, Jan. 1975.*

16. *Green, J. E., "Interactions Between Shock Waves and Boundary Layers," in Progress of Aero. Sci., Vol. 11, Pergamon, N.Y., 1965, pp. 319.*

17. *Rose, W. C., Murphy, J. D., and Watson, E. C., "Interaction of an Oblique Shock Wave with a Turbulent Boundary Layer," AIAA Jour. 7, December 1969, pp. 2211-2221.*

18. *Hankey, W. L., and Holden, M. S., "Two-Dimensional Shock Wave-Boundary Layer Interactions in High Speed Flow," AGARDograph 203, June 1974.*

the Reynolds numbers of practical interest. In this regard, we re-emphasize that this deck contains all of the skin friction and incipient separation effects in the interaction, which alone are suficient reasons to examine it in detail. Regarding (b), it is pointed out that application of $Re_\ell \to \infty$ asymptotic theory results (no matter how rigorous in this limit) to ordinary Reynolds numbers is itself an approximation which may be no more accurate, (indeed perhaps less so) than a physically well-constructed non-asymptotic theory. Direct extrapolated-asymptotic versus non-asymptotic theory comparison have definitely shown this to be the case for laminar flows (especially as regards the skin friction aspect[19]) and the situation has been shown to be possibly even worse in turbulent flow[6]. For example, the asymptotic first order theory formally excludes both the streamwise interactive pressure gradient effect on the shear-disturbance deck and both the normal pressure gradient and so-called "streamline divergence" effects on the middle deck; however, physical considerations plus experimental observations and recent comparative numerical studies[20,21] suggest that these effects may in fact be significant at practical Reynolds numbers and should not be neglected. Of course, second order asymptotic corrections can be devised to redress this difficulty but, as Neyfeh and Regab[22] have shown, run the risk of breaking down even worse when extrapolated to ordinary Reynolds numbers. In the present work, we avoid these problems by using a deliberately non-asymptotic triple-deck model appropriate to realistic Reynolds numbers that includes the inner deck pressure gradient terms plus the middle deck $\partial p/\partial y$ and streamline divergence effects, along with some simplifying approximations that render the resulting theory tractible from an engineering standpoint. With this viewpoint in mind, we now examine in more detail the nature of the disturbance flow problem in each of the three basic decks.

B. Formulation of the Disturbance Problem in Each Deck

1. Outer Potential Flow Region. Assuming that the incident shock and its reflection system are weak with isentropic non-hypersonic flow, we have here a

---

19. *Burggraf, O. R., "Asymptotic Theory of Separation and Attachment of a Laminar Boundary Layer on a Compression Ramp," in AGARD CP-168 - Flow Separation, 1975.*

20. *Werle, M., and Bertke, S. D., "Application of an Interacting Boundary Layer Model to the Supersonic Turbulent Separation Problem," University of Cincinnati Report AFL 76-4-21, August 1976.*

21. *Le Balleur, J. C., Peyret, R., and Vivand, H., "Numerical Studies in High Reynolds Number Aerodynamics," in Computers and Fluids, Vol. 8, Pergamon, 1980, pp. 1-30.*

22. *Ragab, S. A., and Nayfeh, A. H., "A Second Order Asymptotic Solution for Laminar Separation of Supersonic Flows Past Compression Ramps," AIAA 78-1132, 1978.*

small disturbance potential inviscid motion imposed upon the undisturbed uniform flow U_{o_e} outside the boundary layer:

$$\left[M_{o_e}^2 - 1 + (\gamma + 1)\, u' \frac{M_{o_e}^2}{U_{o_e}}\right] \frac{\partial u'}{\partial x} \simeq \frac{\partial v'}{\partial y} \tag{1}$$

$$\partial v'/\partial x \simeq \partial u'/\partial y \tag{2}$$

$$\frac{\partial^2 p'}{\partial y^2} + \left[1 - M_{o_e}^2 - 2 \frac{u' M_{o_e}^2}{U_{o_e}}\right] \frac{\partial^2 p'}{\partial x^2} \simeq 0 \tag{3}$$

where the third term within the square brackets of Eqs. (1) and (3) is significant in the transonic regime $1 < M_{o_e} \leq 1.1$ and automatically includes the supersonic-subsonic jump conditions to this order of approximation[23]. Since a variety of efficient analytical or numerical methods are presently available to solve this system in either transonic flow or in purely supersonic flow (in which case Eqs. 1-3 further reduce to an Ackert-type problem), we assume that such a solution may be carried out for all x on the upper region $y \geq \delta_o$ subject to the usual far-field conditions as $y \to \infty$. The remaining disturbance boundary condition that must be supplied along $y = \delta_o$ then couples this solution to the underlying double-deck: it requires that the outer disturbance flow pertain to an effective streamline shape (relative to the wall) defined by the total interactive displacement effect of the inner decks. To insure physically-smooth matching along this outer-inner interface, then, we require both v'/U_{o_e} and p' to be continuous with their middle deck counterparts along $y = \delta_o$.

2. Middle Rotational-Disturbance Flow Deck. This layer contributes to and transmits the displacement effect, contains the boundary layer lateral pressure gradient due to the interaction and carries the significant influence of the incoming boundary layer profile shape. Our analysis of this layer rests on the key simplifying assumption that for non-separating interactions the turbulent Reynolds shear stress changes are small and have a negligible

---

23. *Murman, E. M., and Cole, J. D., "Calculation of Plane Steady Transonic Flow," AIAA Jour. 9, January 1971, pp. 114-121.*

back effect on the mean flow properties along the interaction zone; hence this stress can be taken to be "frozen" along each streamline at its appropriate value in the undisturbed incoming boundary layer. This approximation, likewise adopted by a number of earlier investigators with good results, is supported not only by asymptotic analysis[24] but especially by the results of Rose's several[17,25] detailed experimental studies of a non-separating shock-turbulent boundary layer interaction which showed that over the short-ranged interaction length straddling the shock the pressure gradient and inertial forces outside a thin layer near the wall are at least an order of magnitude larger than the corresponding changes in Reynolds stress. Furthermore, there is a substantial body of related experimental results on turbulent boundary layer response to various kinds of sudden perturbations and rapid pressure gradients which also strongly support this view (see Ref. 6). These studies unanimously confirm that, at least for non-separating flows, significant local Reynolds shear stress disturbances are essentially confined to a thin sublayer within the Law of the Wall region (see below) where the turbulence rapidly adjusts to the local pressure gradient, while outside in the Law of the Wake region the turbulent stresses respond very slowly and remain nearly frozen at their initial values far out of local equilibrium with the wall stress.

Confining attention, then, to the short range local shock interaction zone where the aforementioned "frozen turbulence" approximation is applicable, the disturbance field caused by a weak shock is one of small rotational inviscid perturbation of the incoming non-uniform turbulent boundary layer profile $M_o(y)$, governed by the equations

$$\frac{\partial}{\partial y}\left[\frac{v'(x,y)}{U_o(y)}\right] = \frac{1-M_o^2(y)}{\gamma M_o^2(y)} \cdot \frac{\partial(p'/p_o)}{\partial x} \tag{4}$$

$$\frac{\partial u'}{\partial x} = -\frac{\partial p'/\partial x}{\rho_o(y)\, U_o(y)} - \frac{dU_o}{dy} \cdot \frac{v'}{U_o} \tag{5}$$

---

24. *Yajnik, A., "Asymptotic Theory of Turbulent Wall Boundary Layer Flows," JFM 42, 1970, pp. 411-427.*

25. *Rose, W. C., and Childs, M. E., "Reynolds Shear Stress Measurements in a Compressible Boundary Layer within a Shock Wave-Induced Adverse Pressure Gradient," JFM 65, 1, 1974, pp. 177-188.*

$$\frac{\partial^2 p'}{\partial y^2} - \frac{2}{M_o}\frac{dM_o}{dy}\frac{\partial p'}{\partial y} + \left[1-M_o^2 - \frac{2\,u'M_o^2}{U_o}\right]\frac{\partial^2 p'}{\partial x^2} = 0 \qquad (6)$$

where Eq. (4) is a result of the combined particle-isentropic continuity, x-momentum and energy equations. It is noted that, consistent with the assumed short range character of the interaction, the streamwise variation of the undisturbed turbulent boundary layer properties that would occur over this range are neglected, taking $U_o(y)$, $\rho_o(y)$ and $M_o(y)$ to be arbitrary functions of y only with δ_o, δ_o^* and τ_{w_o} as constants. Now Eq. (6) is a generalization of Lighthill's well-known pressure perturbation equation for non-uniform flows[8] which includes a non-linear correction term for possible transonic effects within the boundary layer including the diffracted impinging shock above the sonic level of the incoming boundary layer profile. Excluding the hypersonic regime, Eqs. (4)-(6) therefore apply to a wide range of initially supersonic external flow conditions and the complete speed range across the boundary layer except at the singular point $M_o \to 0$ (which we avoid by consideration of the inner deck as shown below). In particular, use of Eq. (6) provides an account of any lateral pressure gradient that develops across the interacting boundary layer.

As is the case with the outer deck, a variety of analytical or numerical methods may be used to solve this middle deck disturbance problem (see e.g., Refs. 8, 10, 17). Whatever the method chosen, we imagine that it provides at each streamwise station x an evaluation of the disturbance pressure distribution p'(x,y); then y-integration of Eq. (4) gives

$$\frac{v'(x,y)}{U_o(y)} = \underbrace{\left[\frac{v'}{U_o}\right](x,y_{w_{eff}})}_{=0} + \frac{\partial}{\partial x}\left\{\int_{y_{w_{eff}}}^{y} \frac{p'}{\gamma p e_1}\left[\frac{1-M_o^2(\bar{y})}{M_o^2(\bar{y})}\right] d\bar{y}\right\} \qquad (7)$$

where $y_{w_{eff}} > 0$ is the effective wall shift or displacement height associated with the inner deck defined such that the inviscid $v'(x,y_{w_{eff}})$ and hence $\partial p'/\partial y(x,y_{w_{eff}})$ both vanish (see below). Equation (7) provides the disturbance streamline slope distribution across the boundary layer at any streamwise station, and its value at $y = \delta_o$ yields the total streamline displacement effect of the two inner decks (the lower limit on the integral being the inner deck contribution). We then may obtain the corresponding total displacement thickness growth along the interaction by streamwise-quadrature of the perturbation boundary layer continuity equation integral; this yields to first perturbation

$$\Delta\delta^*(x) \simeq \int_{y_{w_{eff}}}^{\delta_o} \frac{p'}{p_{e_1}} \left(\frac{1-Mo^2}{Mo^2}\right) dy + (\delta_o - \delta_o^*) \left[\frac{M_{e_1}^2 - 1}{\gamma M_{e_1}^2 \; p_{e_1}}\right] p_w'(x) \qquad (8)$$

3. The Inner Shear-Disturbance Layer. This very thin inner deck contains the significant viscous and turbulent shear stress disturbances due to the interaction, plus the small upstream influence and an important contribution to the viscous displacement effect. In fact it lies well within the Law of the Wall region of the incoming turbulent boundary layer profile and also (for the high Reynolds numbers of interest here) below the sonic level of the profile as our resulting theory indeed confirms aposteriori. The original work of Lighthill[8] and others treated the problem by further neglecting the turbulent stresses altogether and considering only the laminar sublayer effect; while this greatly simplifies the problem and yields an elegant analytical solution, the results can be significantly in error at high Reynolds numbers and cannot explain (and indeed conflicts with) the ultimate asymptotic behavior pertaining to the $Re_\ell \to \infty$ limit. The present theory remedies this by extending Lighthill's approach to include the entire Law of the Wall region turbulent stress-effects; the resulting general shear-disturbance sublayer theory provides a non-asymptotic treatment which encompasses the complete range of Reynolds numbers. It is noted in this connection that our consideration of the entire Law of the Wall combined with the use of the effective inviscid wall concept to treat the inner deck displacement effect eliminates the need for the "blending layer"[11] that is otherwise required to match the disturbance field in the laminar sublayer region with the middle inviscid deck; except for higher order derivative aspects of asymptotic matching, our inner solution effectively includes this blending function since it imposes a boundary condition of vanishing total shear disturbance at the outer edge of the deck. In addition, our retention of the explicit disturbance pressure gradient term for the inner deck not only provides the correct physics at practical Reynolds numbers but also correctly models the situation near separation ($\tau_w \to 0$) where this term becomes of dominant importance.

To facilitate a tractible theory, we retain only the main physical effects by introducing the following simplifying assumptions. (a) The incoming boundary layer is free from any post-transitional memory or low Reynolds number effects and its Law of the Wall region is characterized by a constant total (laminar plus turbulent eddy) shear stress and a Van Driest-Cebeci type of damped eddy viscosity model[26]. This model is known to be a good one for a wide range of upstream non-separating boundary layer flow histories. (b) For the weak incident shock strengths of present interest, the sublayer disturbance flow is assumed to be a small perturbation upon the incoming boundary

---

26. *Cebeci, T., and Bradshaw, P., "Momentum Transfer in Boundary Layers, McGraw-Hill/Hemisphere," Wash., D. C., 1977, p. 365.*

layer; in the resulting linearized disturbance equations, however, all the physically-important effects of streamwise pressure gradient, streamwise and vertical acceleration, and both laminar and turbulent disturbance stresses are retained. Although the resulting theory necessarily becomes inaccurate near separation, it provides a valuable physical insight to the interactive physics close to the wall for non-separating flow and a firm basis for subsequent improvement. Moreover, it can be shown that the form of the particular set of linear equations used here is in fact unaltered by non-linear effects; hence even the quantitative accuracy of the present theory is expected to be good until rather close to separation. (c) For adiabatic flows at low-to-moderate external Mach numbers, the undisturbed and perturbation flow Mach numbers are both quite small within the shear disturbance sublayer; consequently the treatment of compressibility effects therein can be greatly simplified without any significant error. Thus, the influence of the density perturbations on the sublayer disturbance flow may be neglected altogether, while the corresponding modest compressibility effect on the Law of the Wall portion of the undisturbed profile is quite adequately treated by the Eckert reference temperature method[27] wherein incompressible relations are used based on wall recovery temperature properties. Excluding hypersonic flow this is equivalent in accuracy to (but easier than) the use of Van Driest's compressible Law of the Wall profile[28]. (d) The turbulent fluctuations and the small interactive disturbances are assumed uncorrelated in both the lower and middle decks. (e) The thinness of the inner deck allows the boundary layer-type approximation of neglecting its lateral pressure gradient; the wall pressure distribution $p'_w(x)$ is taken equal to the overlaying pressure perturbation field along the bottom of the middle deck.

Under these assumptions, the disturbance field is governed by the following continuity and momentum equations:

$$\frac{\partial u'}{\partial x} + \frac{\partial v'}{\partial y} = 0 \tag{9}$$

$$U_o \frac{\partial u'}{\partial x} + v' \frac{dU_o}{dy} + (\rho_{w_o}{}^{-1}) \frac{\partial p'_w}{\partial x} = \frac{\partial}{\partial y}\left[\nu_{w_o} \frac{\partial u'}{\partial y} + \varepsilon_{T_o} \frac{\partial u'}{\partial y} + \varepsilon'_T \frac{dU_o}{dy}\right] \tag{10}$$

$$\partial p'/\partial y = 0 \; ; \; p' = p'(x) \simeq p'_w(x) \tag{11}$$

---

27. *Burggraf, O. R., "The Compressibility Transformation and the Turbulent Boundary Layer Equation,"* Jour. of the Aerospace Sci. 29, *1962, pp. 434-439.*

28. *Van Driest, E. R., "Turbulent Boundary Layers in Compressible Fluid,"* Jour. of the Aeronaut. Sci. 18, *March 1951, pp. 145-160.*

where ρ_{w_o} and ν_{w_o} are evaluated at the adiabatic wall recovery temperature and where it should be noted that the kinematic eddy viscosity perturbation ε_T' is being taken into account. The corresponding undisturbed turbulent boundary layer Law of the Wall profile $U_o(y)$ is governed by

$$\tau_o(y) = \text{const.} = \tau_{w_o} = [\mu_{w_o} + \rho_{w_o} \varepsilon_{T_o}(y)] \frac{dU_o}{dy} \tag{12}$$

where according to the Van Driest-Cebeci eddy viscosity model with $y+ = (y \sqrt{\tau_{w_o}/\rho_{w_o}})/\nu_{w_o}$

$$\varepsilon_T = [.41y(1-e^{-y+/A})]^2 \frac{\partial u}{\partial y} \tag{13A}$$

which yields for non-separating flow disturbances that

$$\varepsilon_{T_o} = [.41y(1-e^{-y^+/A})]^2 \frac{dU_o}{dy} \tag{13B}$$

$$\varepsilon_T' \simeq \left(\frac{\partial u'/\partial y}{dU_o/dy}\right) \varepsilon_{T_o} \tag{13C}$$

Here, A is the so-called Van Driest damping "constant"; we used the commonly-accepted value A = 26 although it is understood that a larger value may improve the experimental agreement in regions of shock-boundary layer interaction.[29] Substituting (13c) into (10) we thus have the disturbance momentum equation

$$U_o \frac{\partial u'}{\partial x} + v' \frac{dU_o}{dy} + (\rho_{w_o} - 1) \frac{\partial p_w'}{\partial x} = \frac{\partial}{\partial y} [(\nu_{w_o} + 2\varepsilon_{T_o}) \frac{\partial u'}{\partial y}] \tag{14}$$

from which we see that inclusion of the eddy viscosity perturbation has exactly doubled the turbulent shear stress disturbance term.

---

29. *Jobe, C. E., and Hankey, W. L., "Turbulent Boundary Layer Calculations in Adverse Pressure Gradient Flows," AIAA Paper 80-0136, Pasadena, January 1980.*

We seek to solve Eqs. (9) and (14) subject to the wall boundary conditions $U_o(0) = u'(x,o) = v'(x,o) = 0$ plus an initial condition $u'(-\infty,y) = 0$ requiring that all interactive disturbances vanish far upstream of the impinging shock. Furthermore, at some distance δ_{SL} sufficiently far from the wall, u' must pass over to the inviscid solution u'_{inv} along the bottom of the middle deck, this latter being governed by Eq. (9) plus

$$U_o \frac{\partial u_{inv}}{\partial x} + v'_{inv} \frac{dU_o}{dy} + (\rho_{w_o})^{-1} \frac{\partial p_w}{\partial x} \simeq 0 \tag{15}$$

with δ_{SL} defined as the height where the total shear disturbance (proportional to $\partial u'/\partial y$) of the inner solution vanishes to a desired accuracy.

Following Lighthill[8], it proves convenient to convert the foregoing problem into one involving the normal disturbance velocity field v'(x,y). Differentiating Eq. (14) w.r.t. x, substituting Eq. (9) so as to eliminate u' and then differentiating the result w.r.t.y so as to eliminate p'_w by virtue of Eq. (11), one thus obtains the following fourth-order equation for v':

$$\frac{\partial}{\partial x}\left(U_o \frac{\partial^2 v'}{\partial y^2} - \frac{d^2U_o}{dy^2} v'\right) = \frac{\partial^2}{\partial y^2}\left[(\nu_{o_w} + 2\varepsilon_{T_o}) \frac{\partial^2 v'}{\partial y^2}\right] \tag{16}$$

This differential equation contains a three-fold influence of the turbulent flow: the profile $U_o(y)$, its curvature d^2U_o/dy^2 (non-zero outside the laminar sublayer) and a new eddy disturbance stress term $2\varepsilon_{T_o}$. Equation (16) is to be solved together with (11) and (13b) subject to the wall boundary conditions $v'(x,o) = \partial v'/\partial y(x,o) = 0$. A third condition involving v' is obtained by satisfying the x-momentum equation (14) at the wall; when this is differentiated w.r.t. x and Eq (9) used together with the fact that $\varepsilon_T \to 0$ at $y = 0$ we obtain the non-homogeneous condition

$$\frac{\partial^3 v'}{\partial y^3}(x,o) = -(\mu_{o_w}^{-1}) \frac{d^2 p'_w}{dx^2} \tag{17}$$

The fourth boundary condition is the v' equivalent of the outer inviscid matching requirement (15), which yields $v'(x,\delta_{SL}) = v'_{inv}(x,\delta_{SL})$ with the inviscid solution governed by

$$\frac{\partial}{\partial x}\left(U_o \frac{\partial^2 v'_{inv}}{\partial y^2} - v'_{inv} \frac{d^2 U_o}{dy^2}\right) = 0 \qquad (18)$$

with δ_{SL} pertaining to $\partial^2 v'/\partial y^2 \simeq 0$ (i.e., vanishing total disturbance shear) somewhere within the Law of the Wall region[12]. Once the v'(x,y) field is obtained, the attendant streamwise velocity and disturbance shear stress fields may be found from

$$u' = \int_{-\infty}^{x} \frac{\partial u'}{\partial x}\, dx = - \int_{-\infty}^{x} \frac{\partial v'}{\partial y}\, dx \qquad (19)$$

$$\frac{\tau'}{\mu_{w_o}} = \left(1+2\frac{\varepsilon_{T_o}}{\nu_{o_w}}\right) \cdot \frac{\partial u'}{\partial y} = - \left(1+\frac{2\varepsilon_{T_o}}{\nu_{o_w}}\right) \cdot \int_{-\infty}^{x} \frac{\partial^2 v'}{\partial y^2}\, dx \qquad (20)$$

An important and useful feature of this approach is the definition of an "effective inviscid wall" position (or displacement thickness) that emerges from the asymptotic behavior of v' far from the wall[8]; see Figure 4. As schematically illustrated in Figure 4a, this is defined by the value y_{weff} where the "back projection" of the v_{inv} solution vanishes, this projection being the (generally non-linear) solution curve obtained by inwardly-integrating (18) and (12) in the negative y direction starting at δ_{SL}. Physically, y_{weff} thus represents the total mass defect height due to the shear stress perturbation field and hence the effective wall position seen by the overlying inviscid middle deck disturbance flow. As indicated in Figure 4b, this concept serves to couple the inner and middle deck solutions in a direct physically-obvious way by providing the non-singular inner equivalent slip-flow boundary conditions $\partial p'/\partial y\ (y_{eff}) = v'_{inv}(y_{weff}) = 0$ at $U_o(y_{weff}) > 0$ for the middle deck solution of Eq. (6). In practice, this approach has proven quite useful for treating a variety of interaction problems.

C. Approximate Solution by Operational Methods

An analytical solution is further achieved by assuming small linearized disturbances ahead of, behind and below the nonlinear shock jump plus an approximate treatment[30] of the detailed shock structure within the boundary

---

30. *Inger, G. R., "Shock Wave Penetration and Lateral Pressure Gradient Effects on Transonic Normal Shock-Turbulent Boundary Layer Interactions," AIAA J. 15, August 1977, pp. 1179-1200, plus 16, May 1978, p. 541.*

layer, which gives reasonably accurate predictions for all the properties of engineering interest when $M_1 > 1.05$ (as far as the overall interaction properties are concerned, this non-linear shock jump provision plus the various non-uniform viscous flow effects within the boundary layer reduce the lower Mach number limit otherwise pertaining to the linearized supersonic theory in purely inviscid potential uniform flow). As described in detail in References 6 and 10, the resulting equations can be solved by Fourier transform methods yielding the interactive pressure rise and displacement thickness growth inputs to the above extended theory of the inner-disturbance sublayer. The resulting solution contains all the essential physics of the mixed transonic viscous interaction field for non-separating flows including the upstream influence, the lateral pressure gradient near the shock and the onset of incipient separation; numerous detailed comparisons with experiment[31] have shown that it gives a good account of all the important engineering features of the interaction over a wide range of Mach-Reynolds number conditions.

The matching of the outer two decks with the inner shear-disturbance deck in connection with the Fourier inversion process yields the determination of the upstream influence distance, $\ell_{up} = \kappa_{min}^{-1}$; typical numerical results for it showing the important typical parametric effects of Reynolds number and shape factor can be found in Ref. 6. The solution further yields the inner deck displacement thickness

$$\frac{y_{eff_w}}{\delta_o} \simeq .677 \left[\frac{c_{f_o}}{2} Re_{\delta_o}^2 \left(T_{e_o}/T_w\right)^{1+2\omega}\right]^{-1/3} \left(\kappa_{min}\, \delta_o\right)^{-1/3} \cdot H(T)\, P^{1/3} \qquad (21)$$

and the interactive skin friction relationship

$$\frac{\tau_w'(x)}{\tau_{w_o}} \simeq -\left(\frac{\kappa_{min}}{\lambda}\right)^{2/3} \cdot S(T) \sqrt{\frac{\beta}{C_{f_o}}}\, C_{p_w}\, P^{-2/3} \qquad (22)$$

where

$$P \equiv 3\, \kappa_{min} \left(\int_{-\infty}^{x} p_w'^{3/2}\, dx\right)/\left(2\, p_w'^{3/2}\right) \qquad (23A)$$

$$T \simeq (.41)^2 \left[\frac{C_{f_o}}{2} Re_{\delta_o} \left(T_{e_o}/T_w\right)^{1+2\omega}\right]^{1/3} \left(\kappa_{min}\, \delta_o\right)^{-2/3} \qquad (23B)$$

---

31. *Inger, G. R., "Application of a Shock-Boundary Layer Interaction Theory to Transonic Airfoil Analysis," AGARD CP-291, Colorado Springs, Sep 1980.*

$$\lambda\delta_o = .744\ \beta^{3/4}(C_{f_o}/2)^{5/4}\ Re_{\delta_o}(T_{e_o}/T_w)^{\omega+1/2} \qquad (23C)$$

where the functions H(T) and S(T) are given in Figure 5 and represent the wall turbulence effect on the interactive displacement effect and skin friction, respectively. Figure 5, in fact, is a central result of the general non-asymptotic theory, providing a unified account of the entire Reynolds number range in terms of the single new turbulent interaction parameter T (Eq. 23B): it ranges from the limiting behavior of negligible wall turbulence effect pertaining to Lighthill's theory at $T \to 0$ (lower Reynolds numbers) to the opposite extreme of wall turbulence-dominated behavior at $T \gg 1$ pertaining to an asymptotic-type of theory at vary large Reynolds numbers where the inner deck thickness and its disturbance field become vanishingly small. The relationship between these two heretofore-disparate theories has thus been explained and established: they belong at opposite extremes of a general non-asymptotic theory that describes the transition between them. Another important result emerging from Figure 5 is that the asymptotic trends occurring at very large Reynolds numbers cannot be extrapolated down to ordinary values; doing so can yield appreciable error in the inner deck properties of practical interaction problems. This would appear to explain the success of the Lighthill theory in correlating lower Reynolds number turbulent interactions in spite of the mathematical rigor of asymptotic theory: the former is simply closer to the actual physics and correctly predicts more significant interaction effects and scaling under the decidedly non-asymptotic conditions involved. By the same token, the extreme approximation involved in the $T = 0$ limit significantly breaks down at larger Re_ℓ's pertaining to $T \gg 1$, clearly warranting the use of the present theory to account for the increasing role of the wall turbulence effect on the interaction.

An important and useful final consequence of the foregoing analysis is that it yields an explicit analytical criterion for the onset of incipient separation due to an interactive pressure field; setting $\tau_w = \tau_{w_o} + \tau'_w \simeq 0$, Eq. (22) predicts this to occur when

$$C_{p_w}\left[\frac{2\ C_{p_w}{}^{3/2}/\kappa_{min}}{3\int_{-\infty}^{x}(C_{p_w})^{3/2}dx}\right]^{2/3} \geq \frac{\sqrt{C_{f_o}/\beta}}{S(T)}\left(\frac{\lambda}{\kappa_{min}}\right)^{2/3} \qquad (24)$$

where it is re-emphasized that Cp_w here is the local <u>interactive</u> pressure distribution. Equation (24) bears a general resemblance to a Stratford-type[9] of incipient separation relation for turbulent flow, except that the present formula contains the integrated history effect along the interaction whereas Stratford's result involves purely local properties of C_p and dC_p/dx. It is understood, of course, that the present theory actually breaks down approaching such separation owing to the linearization assumptions and the Van Driest/Cebeci wall turbulence model used; nevertheless, Eq. (24) does give at

least a roughly-correct indication of where this will occur, and indeed does so without containing any adjustable empirical constants.

A computer program has been constructed to carry out the foregoing solution method; it involves the middle-deck disturbance pressure solution coupled to the inner deck by means of the effective wall shift (Eq. 21) combined with an upstream influence solution subroutine. The corresponding local total interactive displacement thickness growth and skin friction are obtained from Eqs. (8) and (22), respectively. If desired the attendant boundary layer shape factor change along the interaction may also be calculated as $H = [\delta^*_o + \Delta\delta^*(x)]/\theta^*(x)$ with θ^* given by an x-wise integration of the overall momentum integral equation for the total local boundary layer since $p(x)$, δ^* and C_f are known. The incoming turbulent boundary layer is treated by the compressible version of a universal composite Law of the Wall - Law of the Wake model due to Walz[32] that not only has a convenient analytical form (see Appendix) but also provides a very general fundamental description of this boundary layer in terms of three arbitrary parameters: preshock Mach number, boundary layer displacement thickness Reynolds number, and the incompressible shape factor H_{i_1}. This enables us to account for the important influence of the upstream flow history (pressure gradient, suction, etc.) on the interaction.

D. Comparisons of the Theory with Experiment

Numerous comparisons of the present theory with experimental data from both wind tunnel and free flight experiments have been documented; a sample is presented in Figure 6 to illustrate the predicted behavior and good agreement for the interactive pressure, displacement thickness and skin friction distributions in a typical non-separating case. Note especially in Figure 6b the lateral pressure gradient that occurs in the vicinity of the shock. Regarding the skin friction comparison shown in Figure 6d, we note that the "experimental" values were actually inferred[7] from measured velocity profiles along the interaction (hence θ^* and δ^*) by means of the 2-D momentum integral equation; considering the well-known uncertainties involved in their experimental set up and this method, combined with the present theory's own limitations, the agreement is considered good as regards both the magnitude and shape of the C_f curve.

Figure 7 shows a comparison of the predicted local shape factor change along an interaction with some ONERA measurements; it is seen that the theory nicely captures the characteristic local peaking of H near the shock foot as well as the overall behavior.

---

32. *Walz, A., "Boundary Layers of Flow and Temperature," M.I.T. Press, Cambridge, Mass., 1969, pp. 113.*

A particularly interesting comparison with some very recent DFVLR-AVA (Gö) experiments[33] is shown in Figure 8, where we compare with measurements along the non-separating interaction zones on two supercritical airfoils. The experimental C_f values were inferred from streamwise boundary layer profile surveys by means of the Ludwig-Tillman relationship

$$C_f = .246(T^*/Te)^{.796}\ Re_{\theta^*}^{-.268}\ e^{-1.561\ H_i} \tag{25}$$

where H_i is given by

$$H_i \simeq (H - .273Me^2)/(1.0 + .1145Me^2) \tag{26}$$

and $T^*/Te \simeq 1 + .14\ M_e^2$ for $\gamma = 1.40$ and $P_r \approx .7$ on an adiabatic wall. Theoretical predictions of the entire airfoil flow field were also made with a composite inviscid transonic - turbulent boundary layer - shock interaction numerical scheme in which the present theory was used as a local interactive module astride the inviscid shock location (see Reference 33 for details). It is seen that the theory yields an excellent prediction of the local skin friction values upstream and slightly downstream of the shock (including the minimum value) and a good qualitative account of the overall shape of the streamwise distribution. Well downstream of the shock, the theory slightly overestimates the post-shock C_f recovery inferred by the Ludwig-Tillman relationship. Nevertheless, in view of the combined limitations of the experimental Ludwig-Tillman method and the present small disturbance theory, the overall agreement with the data is regarded as good.

III. EXTENSION OF THE LOCAL INTERACTION THEORY TO SPINNING AXISYMMETRIC BODIES

A. Fundamental Assumptions

For the high Reynolds number non-separating flows at zero angle of attack which we are considering here, the extension of the foregoing interaction theory to spinning bodies of revolution is based on the following general physical assumptions. (1) The three dimensional relief and spin effects, while altering certain details and quantitative values of the parameters

---

33. *Nandanan, M., Stanewsky, E. and Inger, G. R., "A Computational Procedure for Transonic Airfoil Flow Including a Special Solution for Shock-Boundary Layer Interaction," AIAA Journal Vol. 19, Dec. 81, pp. 1540-46.*

involved, do not fundamentally change the triple deck interaction structure illustrated in Figure 3. Some detailed analysis has shown that this might not be true only for very slender "needle-like" bodies with unrealistically - high spin rates. (2) Being a small scale local event dominated by rapid changes in a direction normal to the inviscid shock, the physics of the interaction is still essentially "two-dimensional" even on a spinning axisymmetric body; the significant effects of the three dimensional geometry and spin enter primarily from their influence on the surrounding large scale inviscid flow, shock location and incoming boundary layer properties ahead of the interaction. (3) Excluding exceedingly slender bodies and/or very low Reynolds number conditions, both the local turbulent boundary layer thickness δ_0 and streamwise scale of the interaction zone (5-7 δ_0) are small enough compared with the local transverse and longitudinal body radii of curvature to permit neglect of the explicit longitudinal and viscous transverse curvature terms in the governing flow equations and to permit retention of the parallel shear flow approximation for the incoming boundary layer as far as the interaction solution is concerned. (4) The body surface and the overlying boundary layer flow are adiabatic.

We now proceed to examine the basic relations upon which the interaction solution rests, to bring out specifically the influence of axisymmetric flow geometry and spin effects.

B. The Inviscid-Disturbance (Middle and Outer Deck) Regions

1. Some Fundamental Relationships. For the case of bodies at zero angle of attack, the general equations governing the attendant circumferentially - invariant ($\partial/\partial\phi = 0$) flow field are as follows when expressed in the body-oriented coordinates shown in Figure 9 (such cordinates have been chosen here because of their convenience in treating the viscous-interaction aspects of the problem):

CONTINUITY
$$\frac{\partial}{\partial x}(\rho u r^{\varepsilon}) + \frac{\partial}{\partial y}(\rho v r^{\varepsilon}) = 0 \quad \begin{cases} \varepsilon = 0, \text{ 2-D} \\ = 1, \text{ Axisymmetric} \end{cases} \tag{27}$$

STREAMWISE MOMENTUM
$$\rho\left(u\frac{\partial u}{\partial x} + v\frac{\partial u}{\partial y} - \frac{\varepsilon}{r}\frac{\partial r}{\partial x}w^2\right) + \frac{\partial p}{\partial x} \simeq \frac{\partial \tau_{xy}}{\partial y} \tag{28}$$

NORMAL MOMENTUM
$$\rho\left(u\frac{\partial v}{\partial x} + v\frac{\partial v}{\partial u} - \frac{\varepsilon}{r}\frac{\partial r}{\partial y}w^2\right) + \frac{\partial p}{\partial y} \simeq 0 \tag{29}$$

CIRCUMFERENTIAL MOMENTUM

$$\rho\left(u\frac{\partial w}{\partial x} + v\frac{\partial w}{\partial y} + \frac{\varepsilon}{r}\frac{\partial r}{\partial x}uw + \frac{\varepsilon}{r}\frac{\partial r}{\partial y}vw\right) \simeq \frac{\partial \tau_{\phi y}}{\partial y} \tag{30}$$

ENERGY CONSERVATION

$$u\frac{\partial p}{\partial y} + v\frac{\partial p}{\partial y} - a^2\left(u\frac{\partial \rho}{\partial x} + v\frac{\partial \rho}{\partial y}\right) = -(\gamma-1)\left[u\frac{\partial \tau_{xy}}{\partial y} + w\frac{\partial \tau_{\phi y}}{\partial y}\right.$$

$$\left. + \frac{\varepsilon}{r}\frac{w^2}{a^2}\gamma p\left(u\frac{\partial r}{\partial x} + v\frac{\partial r}{\partial y}\right)\right] \tag{31}$$

where $a^2 \equiv \partial p/\partial \rho = \gamma p/\rho$, $r = r_B(x) + y\cos\theta_B$ and where for the moment we have included the viscous terms to the boundary layer-order of approximation. These equations are of course supplemented by the thermal equation of state. Note also that Eq. (30) governs the spin-induced circumferential (cross) flow caused by viscous shear in the boundary layer.

We now proceed to obtain an important gas dynamic relationship involving the velocity field components as follows. First we note from continuity (27) that

$$\frac{\partial \rho}{\partial x} = -\frac{r^{-\varepsilon}}{u}\frac{\partial(\rho v r^{\varepsilon})}{\partial y} - \frac{\rho r^{-\varepsilon}}{u}\frac{\partial}{\partial x}(ur^{\varepsilon}) \tag{32}$$

which when substituted into the energy Equation (31) yields the convective derivative of pressure

$$u\frac{\partial p}{\partial x} + v\frac{\partial p}{\partial y} = -\rho a^2\left(\frac{\partial u}{\partial x} + \frac{\partial v}{\partial y}\right) - \frac{\rho a^2 \varepsilon}{r}\left(u\frac{\partial r}{\partial x} + v\frac{\partial r}{\partial y}\right)$$

$$- (\gamma-1)\left[u\frac{\partial \tau_{xy}}{\partial y} + w\frac{\partial \tau_{\phi y}}{\partial y} + \frac{\varepsilon}{r}\frac{w^2}{a^2}\left(u\frac{\partial r}{\partial x} + v\frac{\partial r}{\partial y}\right)\gamma p\right] \tag{33}$$

Now since the normal and circumferential-flow Mach numbers v/a and w/a, respectively, are very small in the present problem we can hereafter neglect their squares compared with unity with excellent approximation; doing this while substituting $\partial p/\partial x$ from Equation (28) plus $\partial p/\partial y$ from Equation (29) into the LHS of Equation (33), we obtain after some algebra the following equation:

$$\left(1 - \frac{u^2}{a^2}\right)\frac{\partial u}{\partial x} + \frac{\partial v}{\partial y} + \frac{\varepsilon}{r}\left(u\frac{\partial r}{\partial x} + v\frac{\partial r}{\partial y}\right) \simeq \frac{uv\zeta}{a^2} - \left(\frac{u}{p}\frac{\partial \tau_{xy}}{\partial y} + \frac{w}{p}\frac{\partial \tau_{\phi y}}{\partial y}\right) \tag{34}$$

where $\zeta \equiv \partial u/\partial y - \partial v/\partial x$ is the vorticity. Equation (34) is the generalized version of the classical flow equation of compressible inviscid flow which here explicitly accounts for axisymmetric flow effects and the possible presence of vorticity; it thus pertains to flow inside as well as outside the boundary layer.

A second companion equation, of particular use in interaction problems, is the generalized streamline slope relationship obtained by substituting $\partial u/\partial x$ from Equation (28) into the RHS of Equation (33) and rearranging the result into an equation governing v/u; again dropping terms of order $(v/a)^2$ and $(w/a)^2$, we get

$$\frac{\partial(v/u)}{\partial y} + \frac{v}{u}\left[\frac{\partial p/\partial y}{\gamma p} + \frac{\varepsilon}{r}\frac{\partial r}{\partial y}\right] + \frac{\varepsilon}{r}\frac{\partial r}{\partial x} \simeq$$

$$\frac{\left\{\left(1 - \frac{u^2}{a^2}\right)\frac{\partial p}{\partial x} - \left[1 + (\gamma - 1)\frac{u^2}{a^2}\right]\frac{\partial \tau_{xy}}{\partial y} - (\gamma - 1)\frac{wu}{a^2}\frac{\partial \tau_{\phi y}}{\partial y}\right\}}{\gamma p\,(u^2/a^2)} \tag{35}$$

Equation (35) enables one to calculate v/u across the flow by appropriate integration of the pressure and viscous stress-gradient effects including the 3-D relief effect from the last LHS term.

A third important relationship governs the pressure field in a vortical but otherwise negligible shear stress region of flow. This we obtain by dropping the explicit stress terms in solving Equation (35) for $\partial p/\partial x$ and then differentiating the result to obtain, after re-use of Eq. (35), an expression for $\partial^2 p/\partial x^2$; this expression is then subtracted from the result of differentiating Eq. (29) w.r.t.y. After much algebra involving the repeated use of Eqs. (28), (29) and (35) plus the neglect of all v^2/a^2 terms we ultimately obtain

$$\left(1 - \frac{u^2}{a^2}\right)\frac{\partial^2 p}{\partial x^2} + \frac{\partial^2 p}{\partial y^2} - 2\left(\frac{v}{u}\right)\frac{u^2}{a^2}\frac{\partial^2 p}{\partial x \partial y} - \frac{\partial p}{\partial x}\left[\frac{\frac{\partial}{\partial x}\left(\frac{u^2}{a^2}\right)}{u^2/a^2} + \left(1 - \frac{u^2}{a^2}\right)\frac{\partial p/\partial x}{\gamma p}\right.$$

$$\left. - \frac{v}{u}\left(\frac{u^2}{a^2}\frac{\partial u}{\partial y} - \varepsilon\frac{\partial r/\partial y}{r}\right)\right] - \frac{\partial p}{\partial y}\left[\frac{\frac{\partial}{\partial y}\left(\frac{u^2}{a^2}\right)}{u^2/a^2} + \left(\frac{\gamma - 1}{\gamma p}\right)\frac{\partial p}{\partial y} - \frac{\varepsilon}{r}\frac{\partial r}{\partial y}\right.$$

$$\left. - \frac{v}{u}\left(2\gamma\frac{u^2}{a^2} - 1\right)\frac{\partial p/\partial x}{\gamma p}\right] \simeq \varepsilon\frac{u^2}{a^2}\gamma p\left[\frac{\partial}{\partial x}\left(\frac{\partial r/\partial x}{r}\right) - \left(\frac{\partial r/\partial x}{r}\right)^2\right.$$

$$\left. + \frac{v}{u}\left(\frac{2}{r}\frac{\partial^2 r}{\partial x \partial y} - \frac{3\frac{\partial r}{\partial x}\frac{\partial r}{\partial y}}{r^2}\right)\right] \tag{36}$$

This equation constitutes a very generalized form of Lighthill's famous pressure field equation extended here to include arbitrary non-parallel ($v, \partial u/\partial x \neq 0$) vortical shear flows on 2-D or spinning* axisymmetric bodies.

Equations (34), (35) and (36) comprise a trio of basic relations which govern the total interactive flow field in the combined outer-middle deck regions. We now specialize them to apply to the interactive disturbance field by imagining that the flow consists of an incoming turbulent boundary layer plus an overlying inviscid transonic flow (subscript "o") which is slightly perturbed by the interaction caused from a weak nearly-normal shock standing in the outer flow; we thus write $u = U_o + u'(x,y)$, $v = v_o + v'$, $w = w_o + w'$, $\rho = \rho_o + \rho'$ and $p = p_o + p'$ where the primed quantities denote these interactive perturbations. Substituting these perturbation expressions into Eq. (34), neglecting all shear stress disturbances by virtue of the "frozen turbulence" approximation, assuming there is negligible correlation between turbulent fluctuations and these perturbations, and subtracting out the undisturbed flow equations and linearizing the resulting small perturbation-flow equations except for the appropriate transonic terms, we ultimately get the following disturbance flow velocity equation:

$$\frac{\partial v'}{\partial y} + \left[1 - M_o^2 - \frac{u'}{U_o}(\gamma + 1) M_o^2\right] \frac{\partial u'}{\partial x} + \frac{\varepsilon}{r}\left(u' \frac{\partial r}{\partial x} + v' \frac{\partial r}{\partial y}\right)$$

$$- \frac{u'}{U_o}\left[(1 + \gamma) M_o^2 \frac{\partial U_o}{\partial x} + \frac{U_o}{p_o}\left(\frac{\partial \tau_{xy}}{\partial y}\right)_o - \frac{p'}{p_o}\left[U_o \left(\frac{\partial \tau_{xy}}{\partial y}\right)_o\right.\right. \qquad (37A)$$

$$\left.\left. + w_o \left(\frac{\partial \tau_{\phi y}}{\partial y}\right)_o\right] \simeq M_o \zeta_o \left[\frac{v'}{a_o} + \frac{v_o}{a_o}\left(\frac{v_o}{U_o} + 2\frac{a'}{a_o} + \frac{\zeta'}{\zeta_o}\right)\right]\right]$$

where for zero angle of attack $w' = 0$ since the shock position is independent of ϕ and hence the resulting interaction field cannot induce any circumferential cross flow regardless of spin. Now in a typical transonic flow field outside the inner deck, the terms of the last square bracket on the LHS of (37A) are very small compared with the remaining ones and hence may be neglected; likewise, the terms proportional to v_o/a_o are negligiably small compared with v'/a_o. Consequently to the leading order of approximation, Eq. 37A may be simplified to

---

*The spin here is implicit, of course, since all the explicit spin terms are of negligible order w^2/a^2 and hence have been dropped.

$$\frac{\partial v'}{\partial y} + \left[1 - M_o^2(y) - (\gamma+1) M_o^2 \frac{u'}{U_o}\right] \frac{\partial u'}{\partial x} + \frac{\varepsilon}{r}\left(u' \frac{\partial r}{\partial x} + v' \frac{\partial r}{\partial y}\right)$$

$$\approx M_o(y)\zeta_o(y)\frac{v'}{a_o(y)} \tag{37B}$$

which is seen to be a generalized transonic small disturbance equation for either a 2-D or axi-symmetric rotational perturbation field in a parallel background flow $M_o(y)$. Proceeding in a similar manner, the application of Eq. (35) to the small disturbance field yields the following approximate linearized expression governing the perturbation streamline slope v'/U_o:

$$\frac{\partial(v'/Uo)}{\partial y} + \frac{\varepsilon}{r}\frac{\partial r}{\partial y}\frac{v'}{U_o} \approx \frac{\partial p'/\partial x}{\gamma p_o M_o^2(y)}\left[1 - M_o^2(y) - (\gamma-1)\frac{u'}{U_o}\right] \tag{38}$$

while the comparable perturbation version of (36) is found to be

$$\left[1 - M_o^2(y) - (\gamma+1)\frac{u'}{U_o}M_o^2\right]\frac{\partial^2 p'}{\partial x^2} + \frac{\partial^2 p'}{\partial y^2} - \left(2\frac{dM_o/dy}{M_o} - \frac{\varepsilon}{r}\frac{\partial r}{\partial y}\right)\frac{\partial p'}{\partial y}$$

$$\approx \varepsilon\gamma p_o M_o^2(y)\left\{\left[\frac{p'}{p_o} + (\gamma+1) M_o^2 \frac{u'}{U_o}\right]\left[\frac{\partial}{\partial x}\left(\frac{\partial r/\partial x}{r}\right) - \left(\frac{\partial r/\partial x}{r}\right)^2\right]\right. \tag{39}$$

$$\left. + \frac{v'}{U_o}\left[\frac{2}{r}\left(\frac{\partial^2 r}{\partial x \partial y}\right) - 3\left(\frac{\partial r/\partial x}{r}\right)\left(\frac{\partial r/dy}{r}\right)\right]\right\}$$

where the RHS here is evidently a kind of accoustical source-disturbance associated uniquely with the 3-D geometry in a compressible flow.

Equations (37B), (38) and (39) are the three basic equations governing the transonic interactive-small disturbance field (u', v', p') in both the outer and middle decks on either 2-D or spinning axi-symmetric bodies at zero angle of attack. They offer the advantage that the three-dimensional effects appear explicitly and hence their influence can be assessed directly.

2. Influence of 3-D Effects. In preparation for examing these interaction equations, we first evaluate certain terms that appear in the coefficients. Using $r = r_B(x) + y\cos\theta_B$ with r_B the body radius and $\tan\theta_B = dr_B/dx$, we obtain

$$\frac{\partial r/\partial x}{r} = r^{-1} \tan\theta_B \left[1 - (r - r_B) \frac{d\theta_B}{dx}\right] \tag{40A}$$

$$\simeq \sin\theta_B / r_B \qquad \text{near body} \tag{40B}$$

$$\simeq - \frac{d\theta B}{dx} \tan\theta_B \qquad \text{far from body} \tag{40C}$$

and

$$\frac{\partial r/dy}{r} \simeq \cos\theta_B / r \tag{41}$$

Now consistent with our previous neglect of longitudinal curvature terms in the governing equations, we may also neglect such terms here (i.e., those $\sim d\theta_B/dx$); thus $r^{-1}\ \partial r/\partial x$ has at most the "near body" value (40B) while being considered negligible in the far field according to (40C). Using Eqs. (40) and (41) we further obtain the estimates

$$\frac{\partial}{\partial x}\left(\frac{\partial r/\partial x}{r}\right) - \left(\frac{\partial r/\partial x}{r}\right)^2 \simeq -2 r_B^{-2} \sin^2 \theta_B \qquad \text{near body} \tag{42A}$$

$$\simeq 0 \qquad \text{in far field} \tag{42B}$$

and

$$\frac{2}{r} \frac{\partial^2 r}{\partial x \partial y} - \frac{3}{r^2} \frac{\partial r}{\partial x} \frac{\partial r}{\partial y} \simeq - 3 r_B^{-2} \sin\theta_B \cos\theta_B \qquad \text{near body} \tag{43A}$$

$$\simeq 0 \qquad \text{in far field} \tag{43B}$$

where we note that for body regions where $\theta_B \ll 1$ the values given by Eqs. (42) and (43) are very small indeed.

Now consider the transonic small perturbation Equation (37B), which we note includes shock jump effects via the non-linear term $(\gamma + 1)\ M_o^2 \frac{u'}{U_o} \frac{\partial u'}{\partial x}$.

Within the near field region $y \leq \delta_o$ pertaining to the middle deck, we have the order of magnitude estimates that

$$\partial v'/\partial y \text{ and } M_o \zeta_o \frac{v'}{a_o} \sim \frac{v'}{\delta_o}$$

$$\frac{\varepsilon}{r}\left(u' \frac{\partial r}{\partial x} + v' \frac{\partial r}{\partial y}\right) \sim \frac{\varepsilon \delta_o}{r_B}\left(\sin\theta_B + \cos\theta_B\right) \frac{v'}{\delta_o} \tag{44}$$

which in turn show that for slender bodies the explicit 3-D term in Eq. 37A is of order δ_o/r_B smaller than the remaining terms and hence can be neglected in the leading approximation for high Reynolds number turbulent boundary layer flows where typically $\delta_o/r_B \leq .05 - .10$. This implies that the important middle deck region is dominated by the two-dimensional aspects of the short-scale interaction. Turning to the intermediate field region $y \sim r_B \sim r$ within the inner portion of the outer deck, we have the order of magnitude estimates that

$$\frac{\partial v'}{\partial y} \sim \frac{v'}{r_B} \tag{45A}$$

$$(\gamma + 1) \frac{\partial u'}{\partial x} \frac{u'}{U_o} M_o^2 \sim \frac{r_B}{\text{Xinter}} \frac{v'}{r_B} \tag{45B}$$

$$\frac{\varepsilon}{r}\left(u' \frac{\partial r}{\partial x} + v' \frac{\partial r}{\partial y}\right) \sim \left(\sin\theta_B + 1\right) \frac{v'}{r_B} \tag{45C}$$

where Xinter is the streamwise scale of the interaction. Since $5 \leq \text{Xinter}/\delta_o \leq 10$ is much smaller than r_B/δ_o in practical applications, we see that the term (45B) is much larger than the other two, again implying as far as Eq. 37B is concerned that the local physics is predominantly two-dimensional when we include the local transonic shock jumps (as indeed we do) in the treatment of the outer deck. In the far field region $y \sim r > \text{Xinter}$ in the outer portion of the outer deck, we estimate that

$$\frac{\partial v'}{\partial y} \sim \frac{v'}{r} \tag{46A}$$

$$(\gamma + 1) \frac{\partial u'}{\partial x} \frac{u'}{U_o} M_o^2 \sim \frac{r}{\text{Xinter}} \frac{v'}{r} \tag{46B}$$

$$\frac{\varepsilon}{r}\left(u' \frac{\partial r}{\partial x} + v' \frac{\partial r}{\partial y}\right) \sim (\sin\theta_B + 1) \frac{v'}{r} \qquad (46C)$$

which for r > Xinter are all of the same magnitude (except for $u'\partial r/\partial x$). Consequently, in this region the explicit radial spreading term $v'\partial r/\partial y$ in Eq. 37B now becomes of the same order as the remaining 2-D terms in governing the inviscid disturbance field; as is well-known the axisymmetric geometry does indeed influence the asymptotic behavior in the far field by increasing the disturbance decay rate over the 2-D result. In the present application, however, where the finer details of this weak far field behavior are not of interest nor of too much consequence as regards the aerodynamic forces and moments, we shall still neglect the explicit 3-D term in the outer deck solution of Eq. 37B. Indeed, any modest errors involved in this approximation are counteracted by the fact that the resulting "locally-2-D" interaction is centered about the correct shock position from the axisymmetric body inviscid solution.

A similar examination of the disturbance streamline relationship (38) using the order of magnitude estimates (40) - (46) yields the same conclusions: the explicit 3-D geometry terms are an order of magnitude smaller than the remaining interaction-effect terms in both the middle deck and near-field portion of the outer deck, and only in the far-field region $y \sim r >$ Xinter of the outer deck (where in fact v' is quite weak) is the 3-D spreading term in (38) important. An examination of the pressure perturbation Eq. (39) again using (40) - (46) shows that the entire RHS is negligibly small for slender bodies regardless of the y scale, the only explicit 3-D term of possible significance being the radial spreading effect in the coefficient of $\partial p/\partial y$ on the LHS. By the aforementioned arguments, this latter effect is important only in the far-field weak-disturbance region of the outer deck.

To summarize, it has been shown that for high Reynolds number transonic flows on slender axisymmetric bodies of practical interest the dominant shock-boundary layer interaction physics is locally two-dimensional except in the weak far-field region of the outer deck where the explicit 3-D spreading-effect terms are influential in determining the asymptotic disturbance decay. Consequentially, to a good engineering approximation in treating the local shock-boundary layer interaction effects on projectile flow fields of practical interest, the 2-D form of the interaction equations (as solved already in Ref. 6) may be used on slender bodies of revolution as well. Indeed, unless the finer details of the far field are of interest (as for example in sonic boom determination) the resulting minor errors are alleviated by the fact that both the coefficients in these 2-D equations and the far-field inviscid shock location fully include the axi-symmetric geometry effects. In a similar vein, it was shown that in practice body spin adds no explicit new terms to the governing equations for flight at zero angle of attack; the only effects (which we fully account for) are those implicit through the spin effect on the boundary layer properties that appear as coefficients in the disturbance equations.

C. The Inner Shear-Disturbance Deck

The extreme thinness of this sublayer immediately justifies the neglect therein of transverse curvature effects [i.e., $r \simeq r_B(x)$], lateral pressure gradients and temperature variations above the adiabatic surface. We may also use the boundary layer-approximation to the shear stress field. Taking the layer to lie within the Law of the Wall portion of the incoming turbulent boundary layer as in the 2-D case, then, the appropriate governing equations of the total interactive flow on a spinning axi-symmetric body at zero angle of attack become:

$$\frac{\partial}{\partial x}(r_B^{\varepsilon}\ u) + r_B^{\varepsilon}\frac{\partial v}{\partial y} \simeq 0 \tag{47}$$

$$u\frac{\partial u}{\partial x} + v\frac{\partial u}{\partial y} - \frac{\varepsilon}{r_B}\frac{dr_B}{dx}w^2 + \rho_{w_o}^{-1}\frac{\partial p}{\partial x} \simeq \frac{\partial}{\partial y}\left[\left(\nu_{w_o} + \varepsilon_{T_{xx}}\right)\frac{\partial u}{\partial y}\right] \tag{48}$$

$$U_o\frac{\partial w_o}{\partial x} + V_o\frac{\partial w_o}{\partial y} + \frac{\varepsilon}{r_B}\left(U_o\frac{dr_B}{dx} + V_o\cos\Theta_B\right)w_o \simeq \frac{\partial}{\partial y}\left[\left(\nu_{w_o} + \varepsilon_{T_{\phi\phi_o}}\right)\frac{\partial w_o}{\partial y}\right] \tag{49}$$

$$\frac{\partial p}{\partial y} \simeq 0;\ p = p_{w(x)} \tag{50}$$

where Eq. (49) governs the distribution of the spin-induced cross flow $w_o(y)$ in the incoming non-interacted boundary layer. Here ρ_{w_o} and ν_{w_o} are the density and kinematic laminar viscosity coefficient, respectively, based on adiabatic wall conditions, ε_{Txx} and $\varepsilon_{T\phi\phi}$ are the streamwise and circumferential eddy viscosity functions, respectively, and the known pressure $p_w(x)$ is given by the solution along the bottom of the middle deck. In the light of the results from previous boundary layer studies on spinning projectiles[1], it will be assumed here (excluding abnormally-high spin rates and/or extremely slender bodies) that neither the axi-symmetric geometry nor spin fundamentally alters the turbulent structure near the wall; accordingly it is sufficient for the present purposes to adopt the isotropic VanDriest-Cebeci eddy viscosity model

$$\varepsilon_{Txx} \simeq \varepsilon_{T\phi\phi} = k^2y^2\left(1 - e^{-y/L_D}\right)^2\sqrt{\left(\frac{\partial u}{\partial y}\right)^2 + \left(\frac{\partial w_o}{\partial y}\right)^2} \tag{51A}$$

with

$$L_D = A\, \nu_{o_w} \left(\tau_{w,TOT}/\rho_{wo}\right)^{-1/2} \tag{51B}$$

$$\tau_{w,TOT} = \sqrt{\tau_{w_x}^2 + \tau_{w_\phi}^2} \tag{51C}$$

where $\tau_{w_x} = \mu_{wo}\,(\partial u/\partial y)_w$, $\tau_{w_\phi} = \mu_{wo}\,(\partial w/\partial y)_w$, k = .41 and A = 26.

Consider first the undisturbed zero pressure gradient flow in the incoming turbulent boundary layer close to the wall. Although the presence of cross flow $w_o(y)$ due to spin alters the usual constancy of total shear across the Law of the Wall region (as can be seen from Eqs. (48) and (49) with $w_o \simeq w_o(0) + w_o'(0)y$, $w_o(0) \simeq \Omega\, r_B$ in the left hand sides), further analysis shows this effect to be negligibly small for the high Reynolds number-spinning slender body flows of practical interest. Hence to a good approximation the undisturbed profiles $U_o(y)$, $w_o(y)$ obey the following relations obtained by integrating Eqs. 48 and 49 after neglecting their left hand sides:

$$\left[\nu_{ow} + \varepsilon_{T_{xx_o}}(y)\right] \frac{dU_o}{dy} \simeq \tau_{w_{xo}}/\rho_{wo} \tag{52}$$

$$\left[\nu_{ow} + \varepsilon_{T_{\phi\phi_o}}(y)\right] \frac{dw_o}{dy} \simeq \tau_{w_{\phi o}}/\rho_{wo} \tag{53}$$

where $\varepsilon_{T_{xx_o}}$ and $\varepsilon_{T_{\phi\phi_o}}$ are given by Eqs. (51) with $U(y) = U_o(y)$ and where the wall stress ratio $\alpha = (\tau_{w_\phi}/\tau_{w_x})_o$ is presumed a known function of $w_B = w_o(0) = \Omega\, r_B$ which vanishes as $w_B \to o$.

We now imagine the shock-boundary layer interaction process to induce small perturbations $u' = u - U_o$, $v' = v$, $p' = p - p_o$ without, however, affecting the cross flow ($w' \simeq o$, see above). Then restricting attention to the non-separating case by linearizing these disturbances in the first approximation and utilizing the parallel shear flow approximation ($Vo = \partial Uo/\partial x \simeq 0$) for the undisturbed flow consistent with Eqs. 52 and 53, Eqs. 47 and 48 yield the following disturbance flow relations:

$$\frac{\partial u'}{\partial x} + \frac{\partial v'}{\partial y} + \frac{\varepsilon}{r_B}\left(u' \sin\theta_B + v' \cos\theta_B\right) \simeq 0 \tag{54}$$

$$U_o \frac{\partial u'}{\partial x} + v' \frac{dU_o}{dy} + \frac{\partial p'}{\partial x} \simeq \frac{\partial}{\partial y}\left\{\left[\nu_{o_w} + \left(\frac{2+\alpha^2}{1+\alpha^2}\right)\varepsilon_{T_o}\right] \frac{\partial u'}{\partial y}\right\} \tag{55}$$

$$\varepsilon_{T_o} = k^2 y^2 \left[1 - \text{EXP}\left(-\sqrt{1+\alpha^2}\, y+/A\right)\right]^2 \sqrt{1+\alpha^2} \tag{56}$$

where

$$\alpha = \frac{dw_o/dy}{dU_o/dy} \tag{57}$$

is a measure of the local spin-induced cross flow angle, which evidently influences the streamwise turbulent stress perturbation field near the surface. Since α for practical spinning projectiles is typically quite small ($\alpha \leq .05$)[1], however, it is seen that its effect ($\sim \alpha^2$) on the inner disturbance solution is negligible: Eqs. (54) thru (56) thus reduce to their non-spinning form.

We now assess the explicit influence of axisymmetry on the inner solution, which as can be seen enters only via the disturbance continuity equation (54). That this influence is negligible for slender bodies over the relatively short streamwise scale Xinter and very small inner deck height scale δ_{SL} can be established by comparing the following order of magnitude estimates of the various terms in Eq. (54):

$$\frac{\partial u'}{\partial x} \sim \frac{u'}{\text{Xinter}} \quad \text{vs.} \quad \frac{\varepsilon}{r_B} U' \sin\theta_B \sim \frac{u'}{\text{Xinter}} \cdot \sin\theta_B \frac{\text{Xinter}}{r_B}$$

$$\frac{\partial v'}{\partial y} \sim \frac{v'}{\delta_{SL}} \quad \text{vs.} \quad \frac{\varepsilon}{r_B} v' \cos\theta_B \sim \frac{v'}{\delta_{SL}} \cdot \frac{\delta_{SL}}{r_B} \tag{58}$$

Clearly, when Xinter/r_B and $\delta o/r_B$ are small, the last terms in Eq. (58) are negligible for slender bodies and Eqs. (54) thru (56) thus reduce to their two-dimensional form (with however the coefficients based on spinning axisymmetric solution values); like the outer and middle decks, the dominant interaction physics of the inner deck is locally two-dimensional.

D. The Overall Displacement Thickness

The integrated continuity equation across the boundary layer region on an axisymmetric body yields the following general expression for the total displacement thickness $\delta^* \equiv \int_o^\delta (1 - \frac{\rho u}{\rho_e U_e})\, dy$ assuming isentropic inviscid flow along the boundary layer edge:

$$\frac{d\delta^*}{dx} = \frac{ve}{ue} + (\delta - \delta^*)\left[\left(\frac{Me^2-1}{\gamma Me^2}\right)\frac{dp_e/dx}{p_e} + \varepsilon \frac{dr_B/dx}{r_B}\right] \tag{59}$$

where ve/ue is the streamline slope at the edge and where the transverse curvature effect in the integrand has been neglected for $\delta/r_B \ll 1$. The corresponding interactive small perturbation part of Eq. (59), using the 2-D version of Eq. (38) integrated across the boundary layer, gives the local interactive displacement thickness increase as

$$\frac{d\Delta\delta^*(x)}{dx} \simeq \frac{ve'}{Ue_o} + (\delta_o - \delta_o^*)\ \frac{Me_1^2-1}{\gamma Me_1^2}\left(\frac{dp_w'/dx}{p_{e_1}}\right) + \varepsilon \frac{dr_B/dx}{r_B}\ (\Delta\delta - \Delta\delta^*) \tag{60A}$$

$$\simeq \left\{ \int_{y_{w,eff}}^{\delta o} \left[\frac{1 - Mo^2(y)}{Mo^2}\right] dy + (\delta_o - \delta_o^*)\left(\frac{Me_1^2 - 1}{\gamma M_e^2}\right) \right\} \frac{dp_w'/dx}{p_{e_1}}$$

$$+ \varepsilon \left(\frac{\Delta\delta - \Delta\delta^*}{r_B}\right) \sin\theta_B \tag{60B}$$

Now the first bracket on the right side of Eq. (60B) contains two contributions from the interactive pressure field; the first involves a Mach number profile integral across the middle deck plus the inner deck contribution from the non-zero layer limit $y_{w,eff}$ as previously explained, whereas the second is a purely inviscid mass flow effect. The last term on the right constitutes a small explicit contribution from the axisymmetric spreading effect which is negligible in our applications because it involves the product of two terms which are both very small in the interaction regions on a slender body at high Reynolds numbers; discarding it thus leaves the two-dimensional form of Eq. (60B) in which axisymmetry and spin effects are implicitly accounted for in the coefficient values of δo, δo^*, Me_1, p_w' and $Mo(y)$.

IV. COMPOSITE VISCOUS-INVISCID FLOW FIELD MODEL

A composite model of the complete flow field around spinning projectiles at supercritical flight speeds has been constructed which utilizes the foregoing shock-boundary layer interaction theory as a locally-imbedded interactive module astride each body shock location (see Figures 1, 3). We now describe the other components of this model and how they are coupled with the interaction zone solution.

A. Inviscid Solution

The inviscid flow calculations are treated by the method developed by Reklis, Sturek, and Bailey[5] involving the numerical solution of the transonic small disturbance equation for the velocity perturbation potential Φ which in cylindrical coordinates is

$$[(1-M_\infty^2) - M_\infty^2 (\gamma+1)\Phi_x]\Phi_{xx} + \Phi_{rr} + \Phi_r/r + \Phi_{\phi\phi}/ r^2 = 0 \qquad (61)$$

This equation is a second order nonlinear partial differential equation of mixed elliptic/hyperbolic type; the type changes to match the physical differences between regions of subsonic and supersonic flow.

Equation (61) generally yields adequate predictions of the inviscid flow about a projectile shape such as that studied here. Certain regions of the flow require some "modeling", however. The wake is simulated by a necked-down extension from the boattail base smoothly-fared into a cylindrical sting over a distance of two calibers; the base flow is thus modeled as an extended sting. A review of free-flight shadowgraphs for projectile shapes at transonic speeds does show the wake flow to follow near the boattail angle for a distance of one to three calibers before turning parallel to the flow direction, but of course the wake vorticity which physically exists is not accounted for. Moreover, this obviously ignores the wake momentum defect and hence the base contribution to the overall drag, as well as slightly over-estimating the pressure rise and hence the boundary layer thickness growth and skin friction drop near the end of the boattail owing to neglect of the base pressure upstream influence. However, for the present purposes where drag prediction is not of primary interest, these shortcomings are not deemed too significant.

In order to develop a "conservative" algorithm to solve this equation special care must be taken at transitions between subsonic and supersonic flow. Non-conservative forms of the algorithm, however, often give better agreement with experiment because the breakdown in conservation approximates the effect of the shock obliquity resulting from shock-boundary layer interaction (see below). The algorithm used here is therefore a non-conservative one for purposes of a first order composite flow model. Consistently, first order boundary condition relations have been used with 120 streamwise grid points along the body length with higher concentration in the corner/shock interaction regions.

B. Boundary Layer Theory

Turbulent boundary layer flow computations were made by an extension of the method originated by Dwyer and Sanders[1,34]. In this technique the boundary layer equations for the conservation of mass, momentum, and energy are solved with an implicit finite difference technique. The solution begins with the development of an approximate boundary layer profile at the tip. The solution is then marched along the body from nose to tail. At each step along the way a two point boundary value system is solved with conditions given at the body surface and at the boundary layer edge. The possibility of body spin is accounted for and care is taken in setting up the difference equations which are solved to maintain differencing in the correct direction to maintain stability. The solution is started at the body nose tip with the assumption that it is a cone and that the boundary layer solution is self similar along rays through the cone tip. This assumption is strictly true only if the flow at the tip is supersonic. Errors will damp out as the solution proceeds down the body, however, and even when the tip is emersed in subsonic flow the starting conditions obtained from this method have been satisfactory. Turbulence is accounted for by use of a turbulent shear stress model with Van Driest damping. This model has proved suitable for use in cases of supersonic flow and is carried over directly to the transonic regime. Although this method of solving the boundary layer equations has been used for cases of supersonic flow over projectiles[1] in the past, this was the first use of Dwyer's method for problems in transonic flow.

C. Imbedded Local Interaction Solutions

The presence of a local compression shock abruptly terminating the local pocket of supersonic flow following both body corners is identified and located by the inviscid solution code and used to call the interaction solution as an interuptive subroutine centered about each such shock location, using the appropriate local pre-shock Mach number from the code as a driving input to the solution. When inserting the interaction we account for the fact that the non-conservative inviscid code gives shock strengths slightly less than the full Rankine-Hugoniot normal shock jump assumed in the interaction solution by correcting the pre-shock Mach number M_1 used in the latter solution to the value pertaining to a slightly oblique attached shock that produces maximum post-shock flow deflection; this method, which is strongly supported by a correlation of experimental evidence by many investigators (see e.g., Ref. 33 and Figure 11), yields

$$M_{1,\text{eff}} \simeq M_1 \sin(90 - 37.8 \sqrt{M_1 - 1}) \qquad (62)$$

---

34. *Dwyer, H. A., and Sanders, B. R., "Magnus Forces on Spinning Supersonic Cones. Part I. The Boundary Layer," AIAA Journal 14, April 1976, p. 498.*

The additional required inputs of the incoming boundary layer displacement thickness and shape factor are given by the aforementioned turbulent boundary layer code that has been simultaneously calculating along the body. The interaction subroutine replaces the boundary layer code over the range of the interaction with a complete description (if desired) of the local small scale interaction wall pressure, displacement thickness and skin friction distribution (such as those shown in Figure 6), plus the final post-interaction values of δ^*, Cf and the (subsonic) inviscid edge conditions needed to restart the turbulent boundary layer code downstream. This method of introducing the interactive solution allows us to account not only for the rapid displacement thickness growth in each interaction but also for the attendant interactive distortion of both the skin friction and profile shape. Moreover, the important influence of these changes on the subsequent boundary layer development downstream is included in appropriate post-interaction reinitialization of the turbulent boundary layer calculation. Consistent with the turbulent boundary layer model employed within the interaction theory to fit the pre-interaction flow conditions, this reinitialization is carried out at the first post-interactive streamwise station by means of the compressible version of Walz's general composite Law of the Wall - Law of the Wake velocity profile model (Appendix A) with the profile parameters chosen to match the post-interactive values of δ^*, C_f and M_e given by the local interaction solution, leaving the wake function and shape factor to take their consequent highly non-equilibrium post-shock values. Given this profile fit, the turbulent boundary layer code then marches downstream.

It should be noted that since the interaction zones on practical artillery shell result from the rapid overexpansion-recompression regions following the ogive-cylinder and ogive-cylinder-boattail junctions (see Figures 1 and 10) the aforementioned general turbulent boundary layer profile model in the interaction module is required to account for the important effect of the rapid shape factor variation along these regions. This implies that a sufficiently large number of small boundary layer x-steps be concentrated in such regions. On the other hand, these corner-zones simplify the flow problem as well: they fix the shock location nearly independently of the viscous displacement-thickness effects. An illustration of this is shown in Figure 12, where typical Navier-Stokes code pressure distribution predictions[35] at different Reynolds numbers are shown to be close to the inviscid result as corroborated by experiment. Thus, in contrast to the case of a supercritical wing where the shock location and strength are unknown a priori and significantly influenced by boundary layer displacement effects (thereby requiring a global viscous-inviscid interaction calculation[36]), the present problem to a very

---

35. *Nietubicz, C. J., Pulliam, T. H., and Steger, J. L., "Numerical Solution of the Azimuthal-Invariant Thin-Layer Navier-Stokes Equations," ARBRL-TR-02227, March 1980. AIAA Paper 79-0010, January 1979.*

36. *Stanewsky, E., Nanandan, N., and Inger, G. R. Proc. AGARD Symposium on "Computation of Viscous-Inviscid Interactions," AGARD CP-291, Colorado Spring, September 1980.*

good approximation can take the shock location given by the purely inviscid solutions without any global iteration.

V. DISCUSSION OF THEORETICAL RESULTS AND COMPARISONS WITH EXPERIMENT

The present composite viscous-inviscid interaction theory has been developed into a global flow field prediction computer code that is fully operational at BRL. It has been exercised on a number of supercritical projectile cases at zero angle of attack, for which experimental data has also been obtained; following a brief description of these experiments, we will present comparisons below. We will also compare with predictions based on a thin-layer Navier-Stokes numerical code used by BRL. Finally, we will show some interaction-effect predictions in the presence of projectile spin.

A. Experimental Data.

To provide a sound validation base for the development of accurate theoretical prediction methods, a concurrent experimental transonic research program on a typical modern projectile shape (Figure 13) was carried out by BRL. The primary experimental data consisted of surface pressure and turbulent boundary layer profile surveys along the aft portion of a non-spinning model obtained during two different types of tests. In the first series, a pressure-tapped three foot long sting-mounted model was tested by Danberg[37] in the NASA Langley Research Center's 8 foot transonic tunnel at a Reynolds number of $13 \times 10^6/M$ over a Mach number range $.8 \leq M_\infty \leq .97$. The boundary layer surveys were made along both the boattail region and some upstream stations on the cylindrical portion using the sting-mounted total head probe shown in Figure 14. In the second test series[38], a one foot long model was surveyed in the Naval Surface Weapons Center White Oak Supersonic Wind Tunnel #2 at $Re_L = 4.5 \times 10^6$ and $M_\infty = .908$ using a Laser-Doppler Velocimeter.

B. Thin-Layer Navier-Stokes Code.

The Navier-Stokes code with which we have compared in this study is the n-invariant or Generalized Axisymmetric version[35]. This code solves the thin-layer Navier-Stokes equations which are cast in strong conservation form. The formulation allows for arbitrary body geometries and is solved using an implicit approximate factorization finite difference scheme. The "thin-layer" approximation used requires $Re \gg 1$; all the viscous terms in the coordinate direction along the body surface are neglected while terms in the near normal

---

37. *Danberg, J.E., Reklis, R.P., and Inger, G.R., "Pressure Distributions and Boundary Layer Profiles on a Yawed Projectile at Transonic Speeds," University of Delaware Technical Report No. 226, Department of Mechanical and Aerospace Engineering, April 1979 (see also AIAA Paper 79-1551, July 1979).*

38. *Nietubicz, C.J., unpublished wind tunnel data. To be published as a BRL Memorandum Report.*

direction to the body are retained. This approximation is used because, due to computer speed and storage limitations, fine grid spacing can only be provided in one coordinate direction (usually taken as the near normal direction) and the grid spacing available in the other two directions is usually too coarse to resolve the viscous terms. The numerical algorithm used is a fully implicit, approximately factored finite difference scheme (more details of the numerical method, algorithm and boundary conditions can be found in Reference 35). The numerical grid used for all the Navier-Stokes computations is shown in Figure 15. The computational region has been extended to four model lengths in front of and four model lengths behind the projectile. The far field boundary has been set at five model lengths. Such an extensive domain is used to eliminate the possibility of any wave reflection back on to the model. The dark band of lines near the model surface results from a clustering of grid lines which are required in order to adequately resolve the boundary layer region. The minimum spacing at the wall was .0002 model diameters, which resulted in at least 3-5 grid points being in the laminar sublayer. The total number of points in the normal direction was 40. There were 78 grid points in the longitudinal direction with clustering taking place at X/D = 3.2 and 5.3, near the ogive and boattail junction, respectively.

C. Comparisons of Theory and Experiment

1. Pressure Distributions. A typical comparison at M_∞ = .95 of the present composite theory prediction vs. that from the parabolized Navier-Stokes code is shown in Figure 16 to illustrate the acceptable accuracy of the inviscid transonic small disturbance theory embodied in the former. Further comparisons between the two methods and with the experimental data are shown in Figures 17 for several other Mach numbers, where is it seen that overall both predictions agree well with the data. The two rapid expansion regions followed by recompression shocks, associated with the body geometry discontinuities, are clearly evident in the theoretical curves and are fairly well modelled by both theories in view of the rapid streamwise changes involved. The slight differences between the two depend somewhat on the mesh sizes used and also on the fact that the shock position of the composite solution has not been iterated with the global boundary layer displacement effect (as explained above) whereas the Navier-Stokes solution automatically includes this effect.

2. Boundary Layer Velocity Profiles. Figure 18 presents comparisons for a typical M_∞ = .94 flight case of the theoretical and measured boundary layer velocity profiles at three stations behind both the ogive-cylinder and the aft cylinder-boattail junctions. Overall, it is seen that the composite and thin-layer Navier-Stokes solutions are in reasonably good agreement with each other and the data as regards the general shape and streamwise-evolution of the boundary layer, although there are some minor detailed differences which, viewed in the light of the customary experimental uncertainties involved, appear minor. As expected, the greatest discrepancies are found at the most aft station near the boattail base where there is very likely some theoretical error due to the crude base-effect model plus some possible experimental inaccuracy due to probe interference effects in the boattail interaction region[37]. Figure 19 presents analogous comparisons illustrating the same conclusions at the slightly higher flight Mach number M_∞ = .97.

3. Displacement Thickness Distributions. Figure 20a illustrates the 2-D displacement thickness growth along the projectile at M_∞ = .94 predicted by the composite theory; it indicates a significant interactive thickening effect across each shock zone, although this is somewhat mitigated (especially on the boattail) by the thinning effect of the preceding sharp expansion regions. In Figure 20b we compare with the thin-layer Navier-Stokes code prediction and with experimental values in the boattail region calculated from the velocity profile data. The two theories are in reasonably good agreement with experiment bearing in mind the joint analytical - experimental uncertainties in the aft part of the boattail. The most notable theoretical difference is that while the composite solution shows a rapid rise in displacement thickness across the first shock location and then a gradual increase until the expansion of the second corner is felt, the Navier-Stokes results show a continuous increase in displacement thickness over the cylinder portion. This difference is attributable to the fact that the displacement thickness is difficult to define in the Navier-Stokes calculation because it does not distinguish the boundary layer per se as does the composite method.

Further comparisons for the lower flight Mach number case M_∞ = .908 are given in Figure 21, showing similar features and good experimental corroboration (especially of the composite theory's predicted interactive δ^*- rise) on the aft part of the cylindrical section as well as on the boattail.

4. Skin Friction Distributions. Although no experimental values are available for comparison, it is nevertheless instructive to examine the theoretical predictions for this important and sensitive property as a means of assessing code performance and the effects of shock-boundary layer interaction including regions of likely incipient shock-induced local boundary layer separation. Indeed, the prediction of skin friction behavior is usually the most demanding test of any theoretical method; this is particularly true in the present application because of the two regions of rapid expansion/compression along the body. Typical results are illustrated in Figure 22 for the M_∞ = .908 case, where it can be seen that both the composite and Navier-Stokes solutions indicate a sharp C_f rise in the expansion zones at both corners followed immediately by rapid C_f decrease in the shock-interaction zone with a subsequent downstream recovery. The composite solution predicts noticeably larger peak values of these maxima and minima then does the Navier-Stokes code; however, part of this difference is seen to be due to the latters' underprediction of the upstream turbulent skin friction level along the ogive section; when this discrepancy is corrected for, the two methods are seen to be in good quantitative (as well as qualitative) agreement, especially considering the severe C_f changes involved.

Similar conclusions may be drawn from the predictions illustrated in Figures 23 and 24 for M_∞ = .94 and .97, respectively. In all these results it can be observed that the shock-boundary layer interaction zones noticeably reduce C_f well downstream of the shock. Moreover, this effect is especially strong in the boattail region where shock-induced local separation appears imminent.

D. Predicted Interaction Effects in the Presence of Spin

Although experimental data and Navier-Stokes calculations for spinning bodies at transonic speeds are presently not available, it is nevertheless interesting to examine the influence of spin on the interactive flow field predicted by the composite viscous-inviscid solution. Accordingly, the effects of increasing spin rate Ω were studied for a typical full scale projectile flight case; the results are presented in Figures 25a-c for the streamwise distributions of boundary layer shape factor, displacement thickness and skin friction as a function of Ω. It is seen that spin rates of 10 to 15 thousand RPM or higher exert a modest but discernible influence that enhances the interactive thickening on both the cylinder and boattail regions, along with an attendant reduction in shape factor and some increase in C_f in the upstream ogive region. It appears questionable, however, whether the magnitude of these spin effects on the interaction could be distinguished within the typical uncertainty level of experimental measurement.

VI. CONCLUDING REMARKS

This report has presented a detailed triple-deck theory of the transonic shock-nonseparating turbulent boundary layer interaction zones on spinning axisymmetric bodies at zero angle of attack. The theory allows a rather general non-equilibrium turbulent boundary layer history upstream of the interaction. We further described the application of this theory as a local interactive model imbedded in a global composite viscous-inviscid transonic flow field prediction method which can handle two or more such interaction zones. Detailed comparisons with both experimental data and thin-layer Navier-Stokes code predictions were presented to verify the accuracy and reliability of the composite method solutions for pressure, displacement thickness, velocity profiles, shape factor and skin friction distributions along the body over a wide range of Mach/Reynolds number conditions.

Desirable improvements in the present work would include extension to the case of small ($\alpha < 3°$-$4°$) angles of attack and better treatment of the aft region near the base to account for the upstream influence and true flow conditions there.

SECANT OGIVE-CYL.-BOATTAIL
$M_\infty = .946$

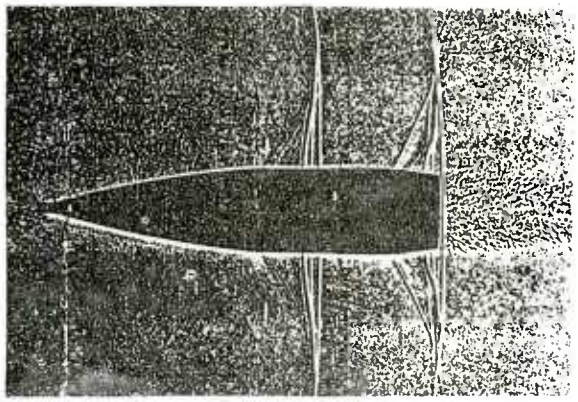

Figure 1. Typical Double-Shock Flow Pattern on a Transonic Projectile

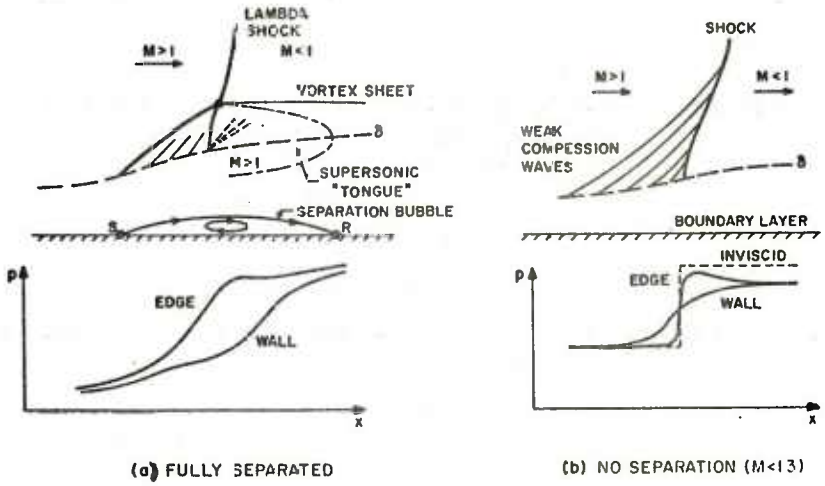

Figure 2. Separated versus Non-Separating Shock-Turbulent Boundary Layer Interaction Patterns

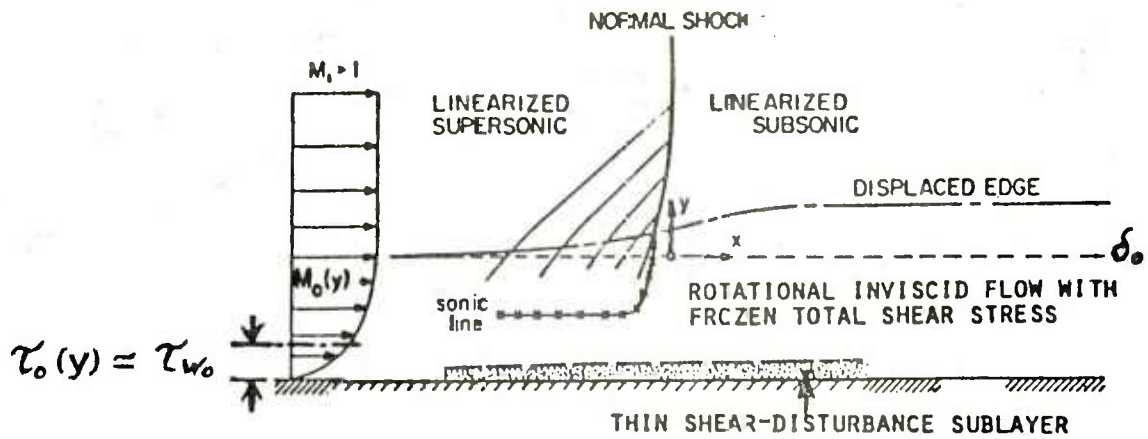

Figure 3. Triple-Deck Structure of the Local Shock Interaction Zone

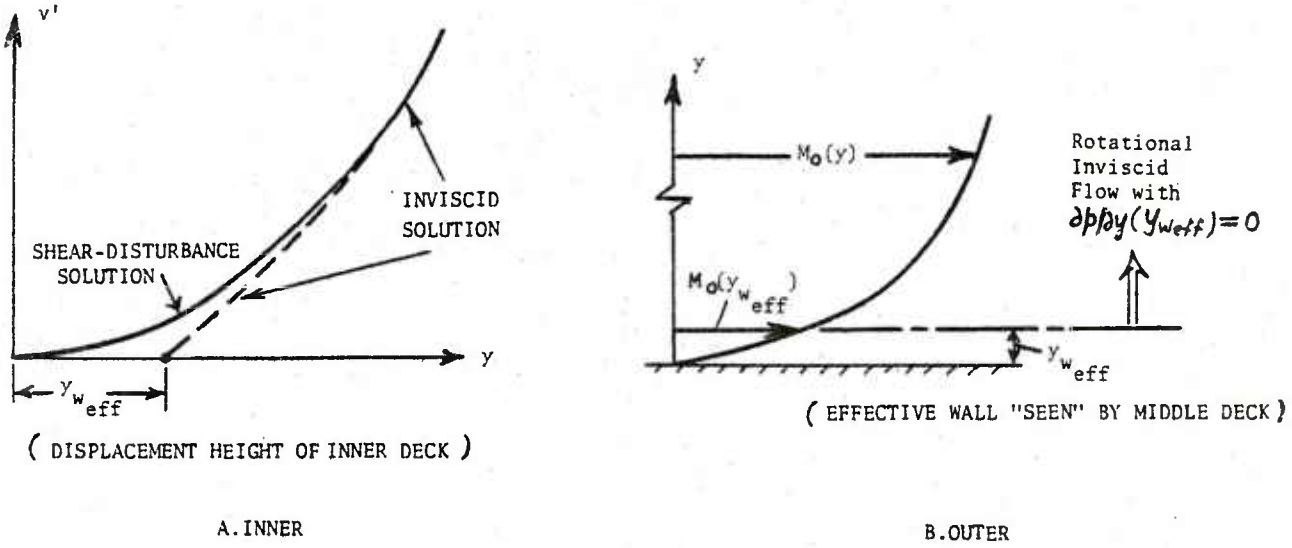

Figure 4. Effective Wall Concept Associated with the Inner Deck Solution (Schematic)

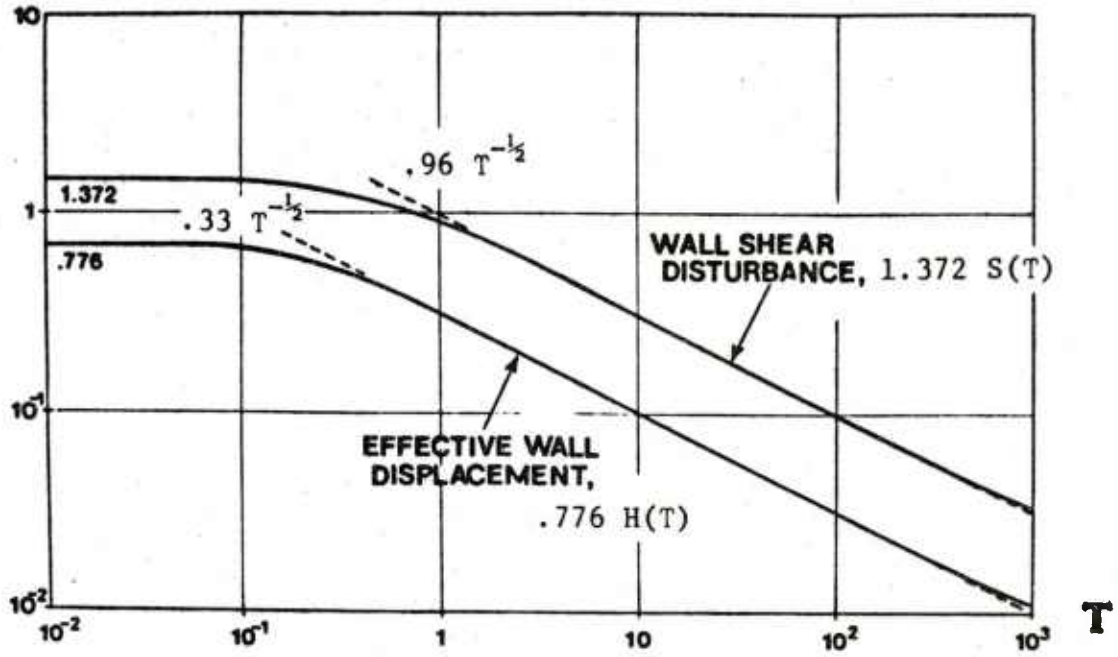

Figure 5. The Displacement Thickness Function H(T) and Disturbance Shear Function S(T)

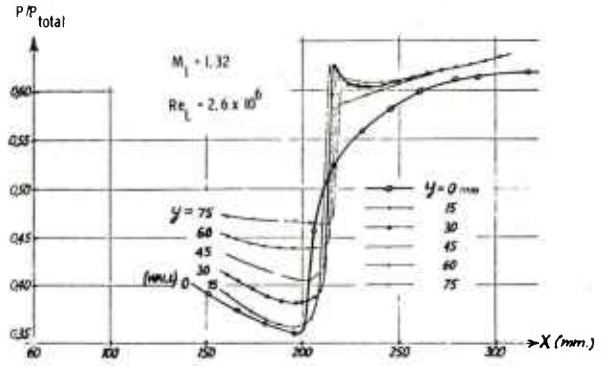

a. Typical Pressure Data

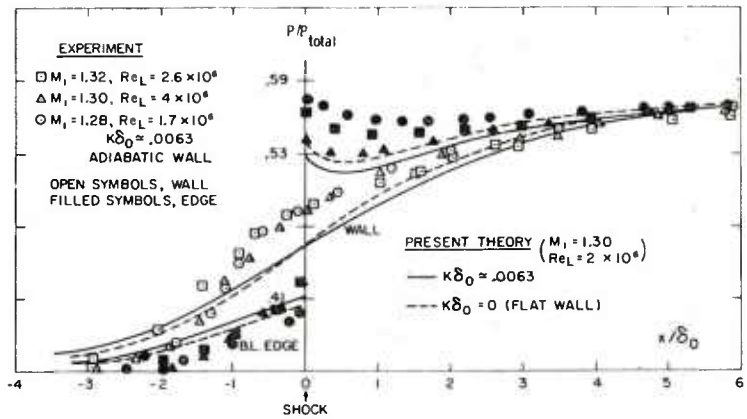

b. Wall and Edge Pressure Comparisons

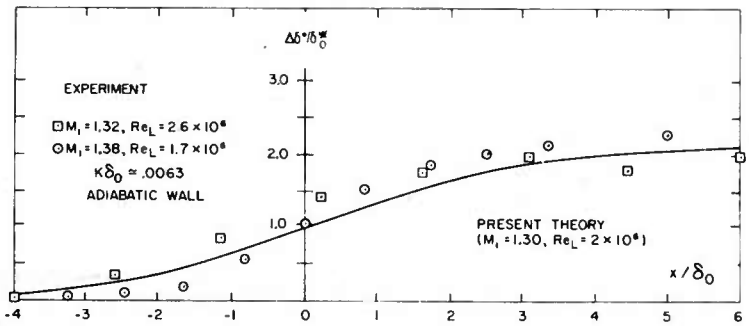

c. Displacement Thickness

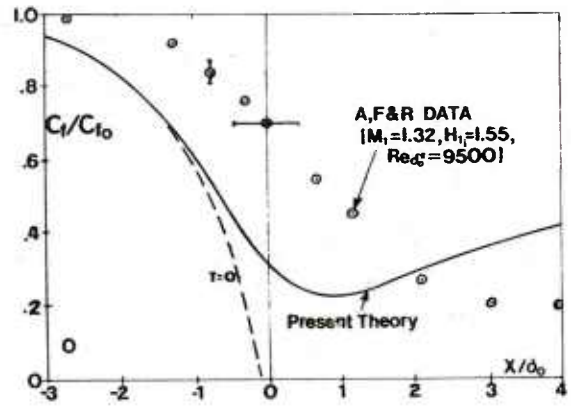

d. Skin Friction

Figure 6. Comparison of Triple-Deck Theory with the Experimental Data of Ackeret, Feldmann and Rott

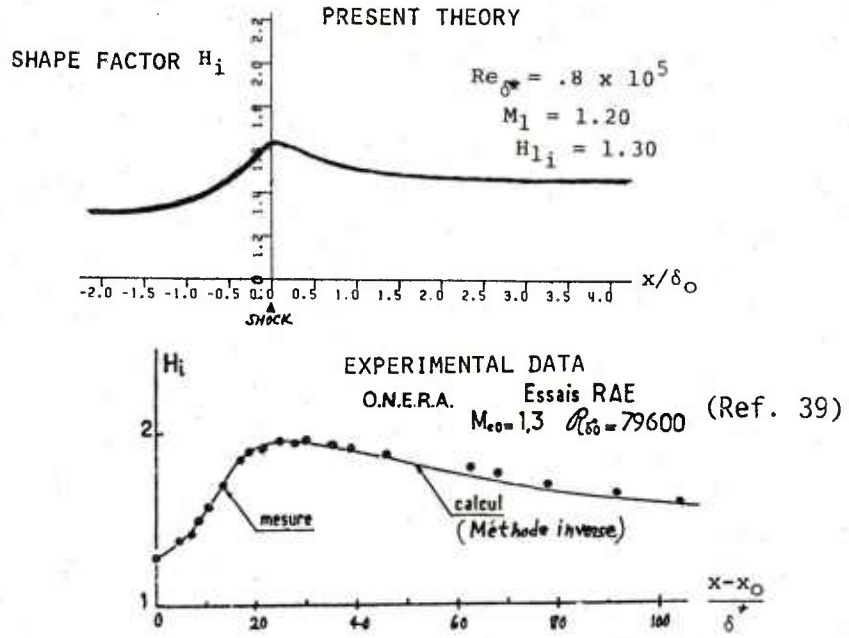

Figure 7. Comparison of the Predicted Interactive Shape Factor Variation with ONERA Data

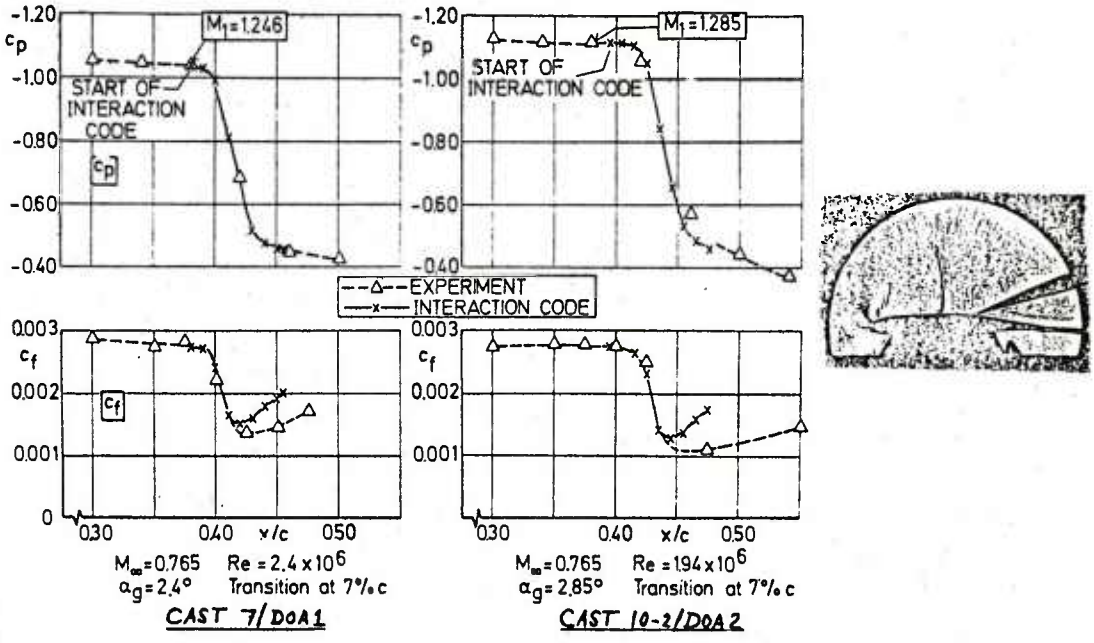

Figure 8. Comparison of Triple-Deck Theory with DFVLR-AVA (Gö) Measurements on a Supercritical Airfoil

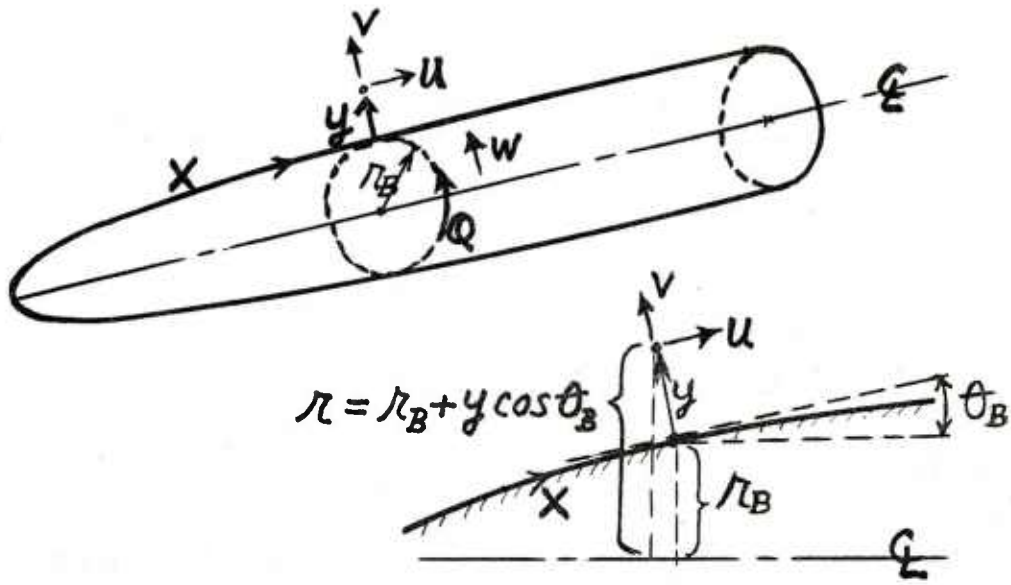

Figure 9. Body-Oriented Coordinate System for Axisymmetric Bodies

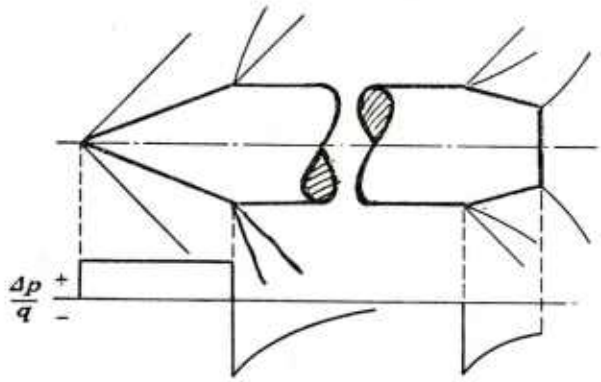

Figure 10. Schematic of the Expansion-Corner Regions

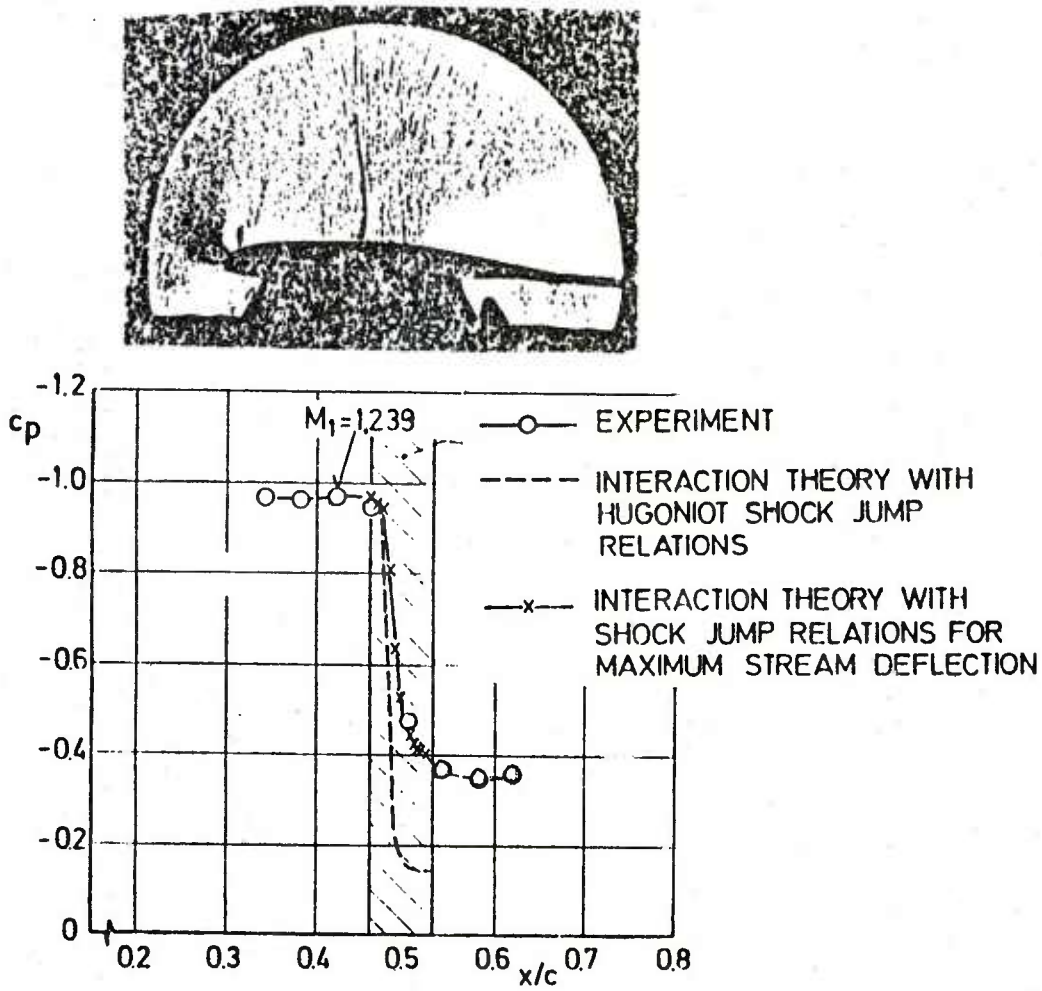

Figure 11. Shock Obliquity Due to Viscous Effects

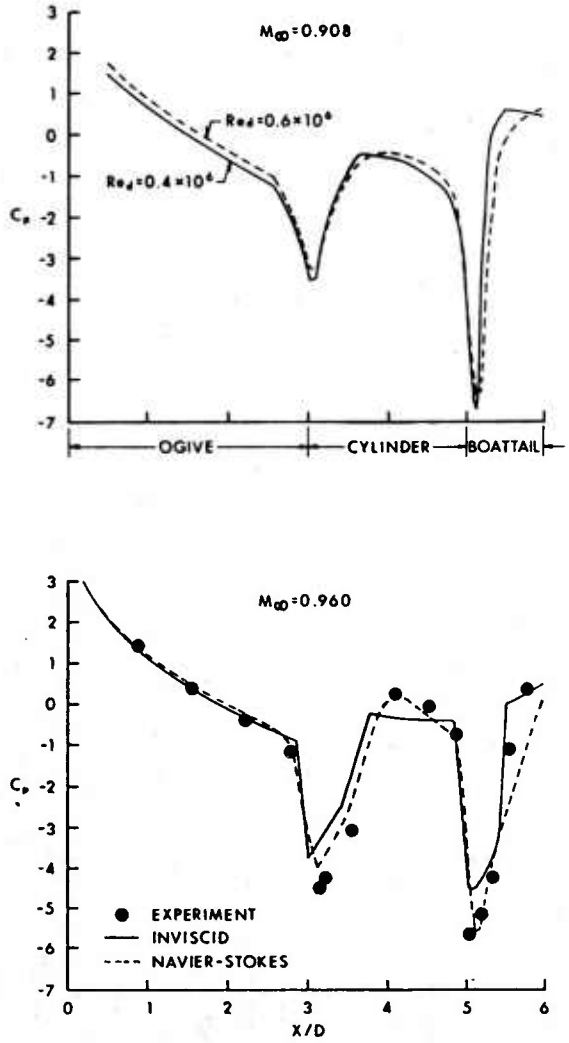

Figure 12. Navier-Stokes Code Pressure Distribution Predictions versus Reynolds Number

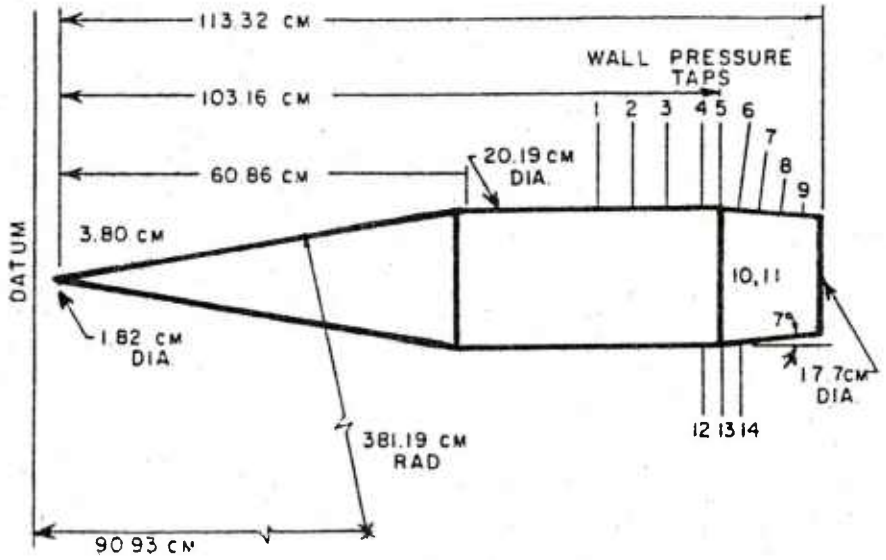

Figure 13. Typical Projectile Model for Experimental Studies

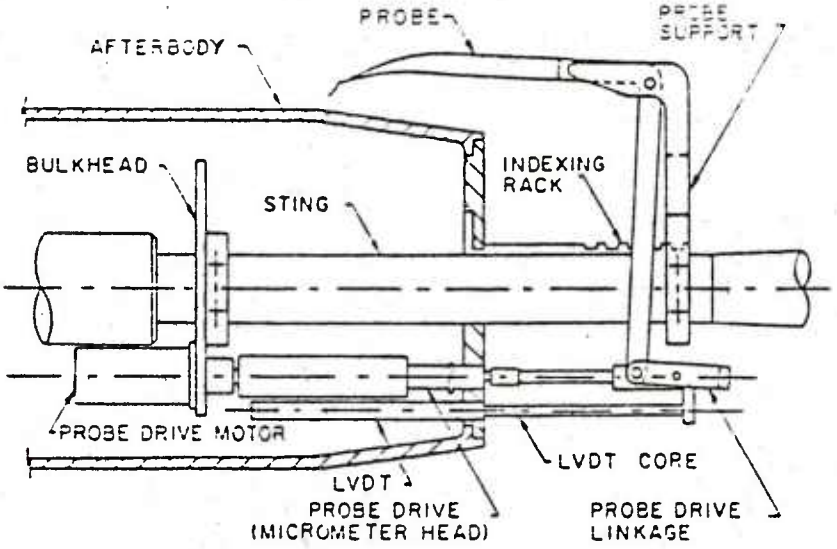

Figure 14. Sting-Mounted Total Head Probe in Danberg's Experiment

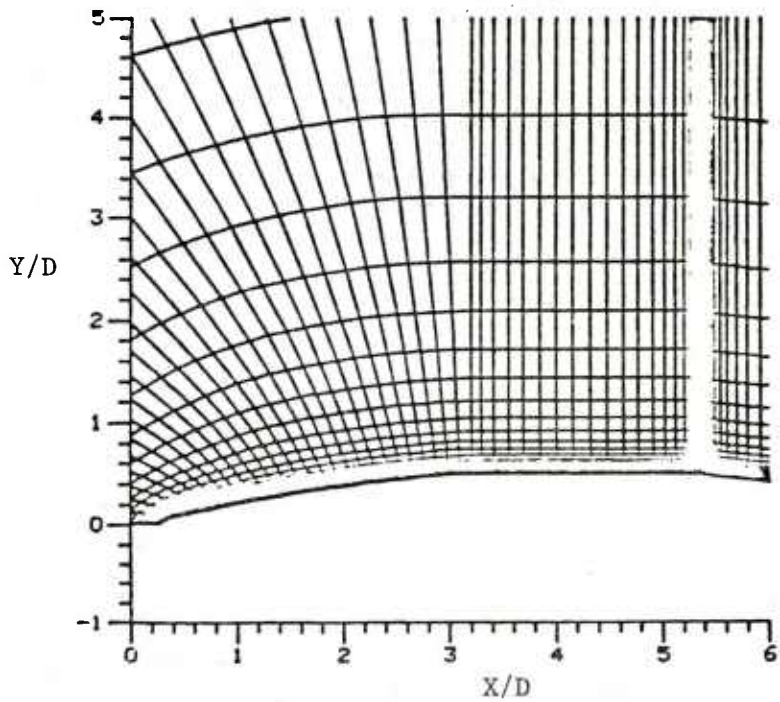

Figure 15. Grid System Used in the Navier-Stokes Calculations of Nietubicz et al (Ref. 35)

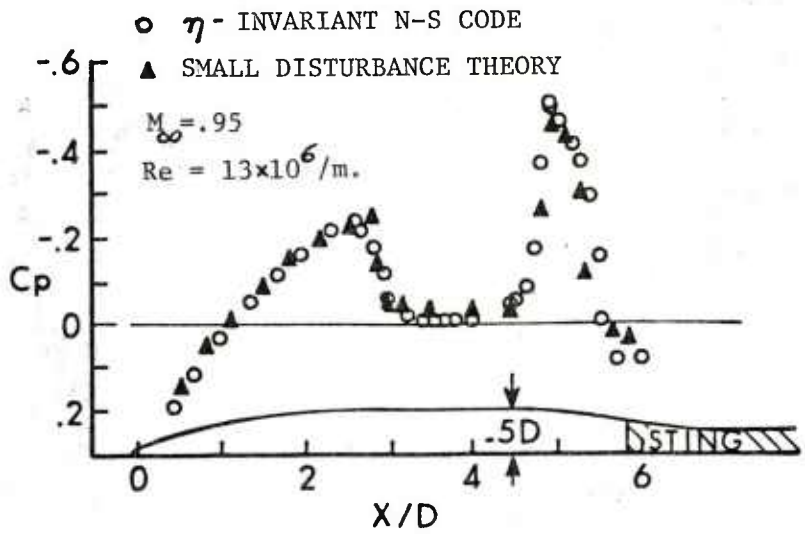

Figure 16. Comparison of Transonic Small Disturbance Theory and Navier-Stokes Predictions of the Axial Pressure Disbribution

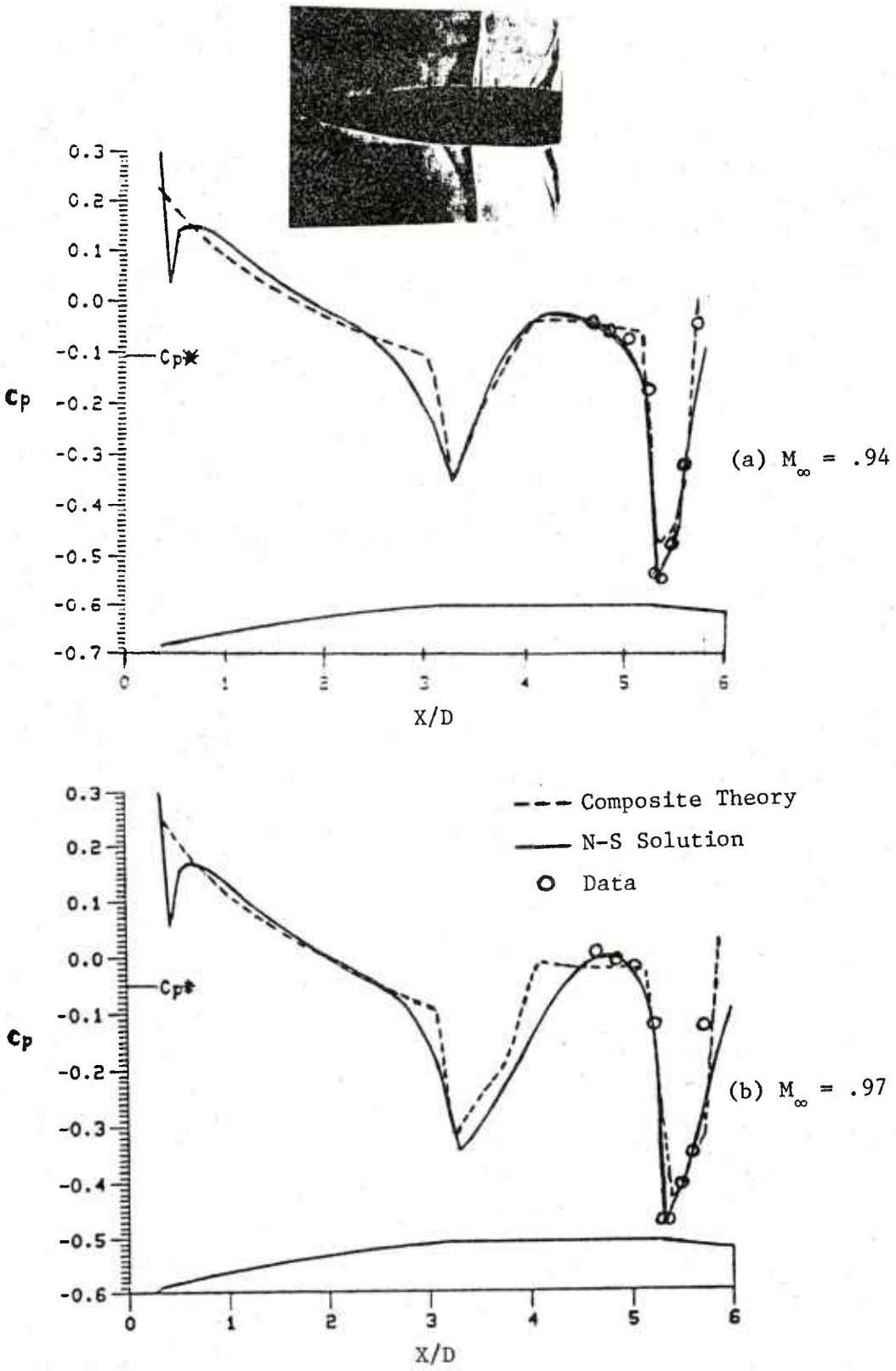

Figure 17. Comparison of Composite Inviscid-Viscous and Navier-Stokes Pressure Distributions versus Experiment

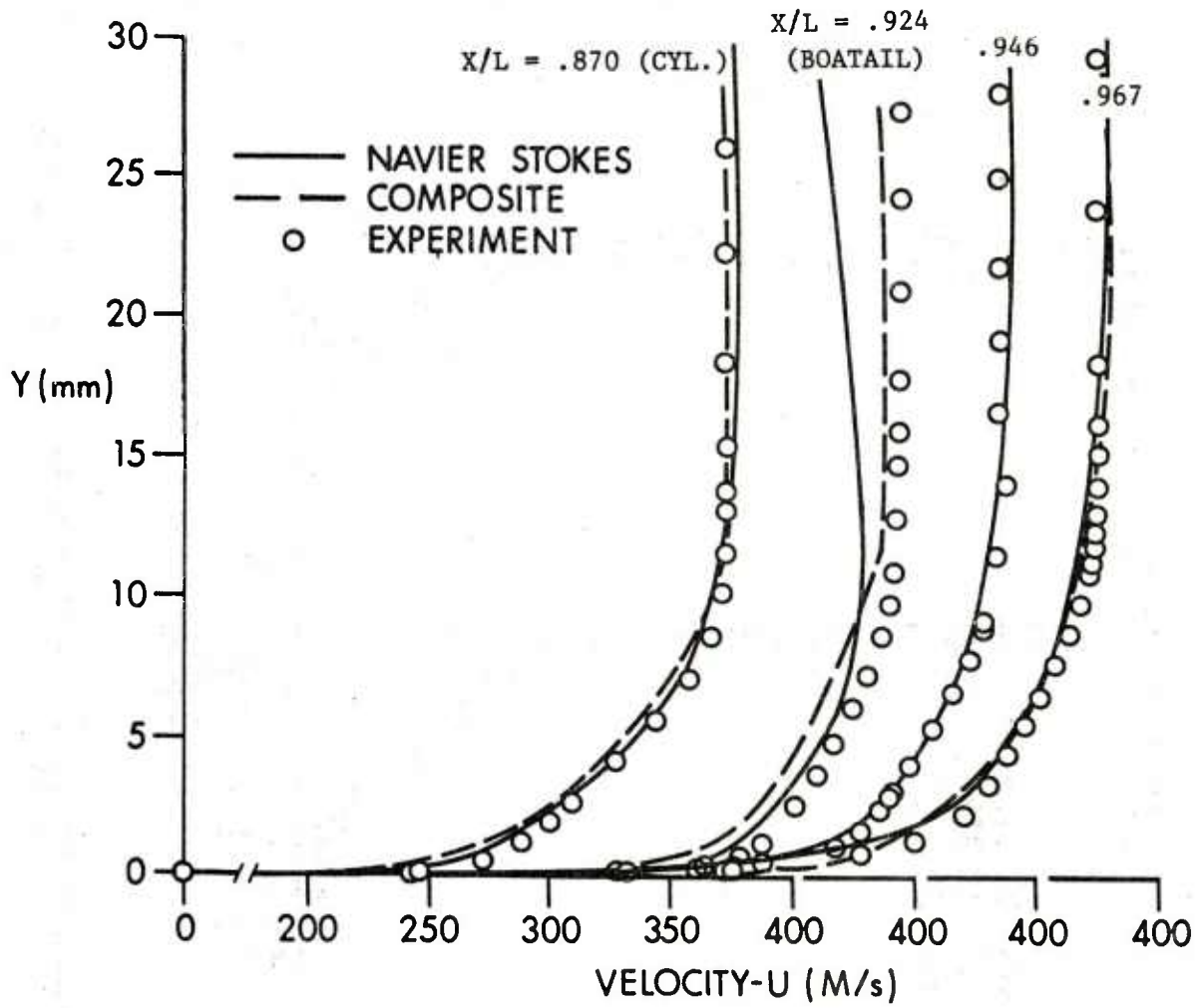

Figure 18. Comparison of Composite Solution, Navier-Stokes and Experimental Boundary Layer Profiles at M_∞ = .94

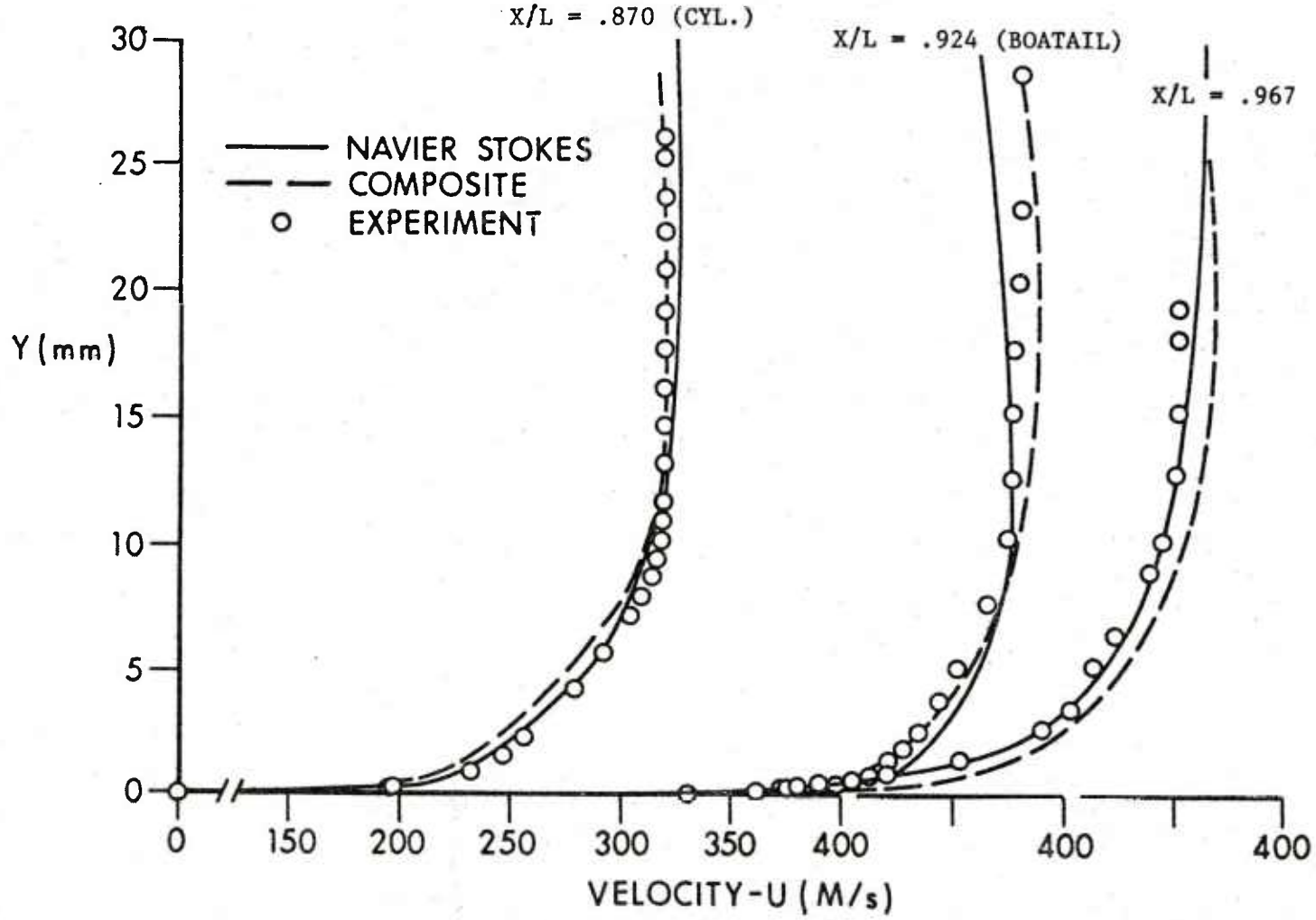

Figure 19. Comparison of Composite, Navier-Stokes and Experimental Boundary Layer Profiles at M_∞ = .97

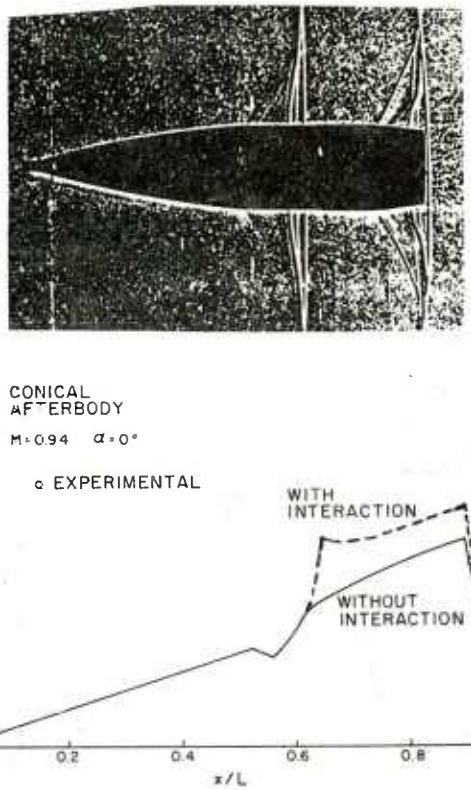

a. Composite Interaction Theory Prediction

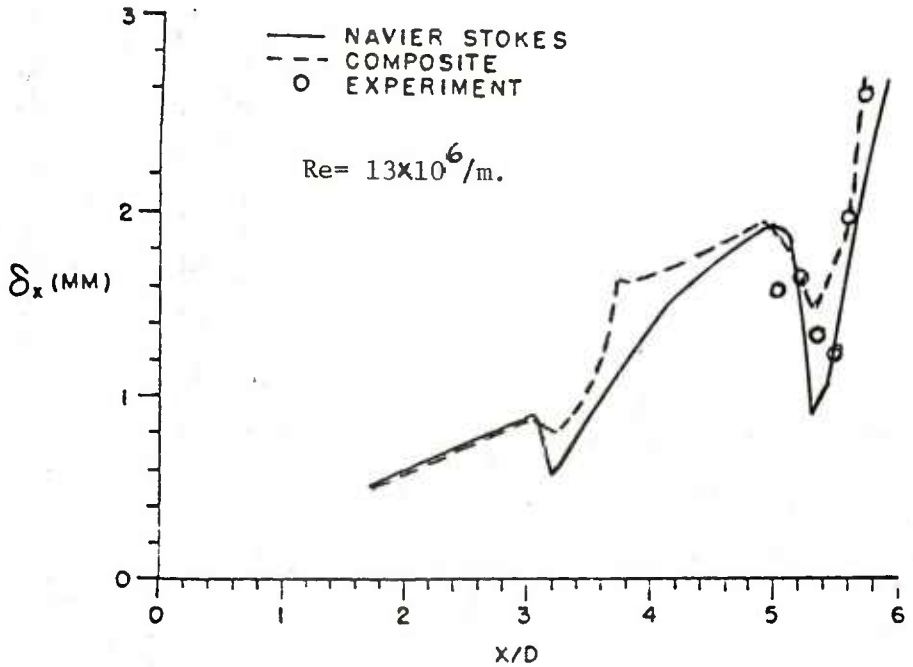

b. Comparison with Navier-Stokes Results and Experimental Data

Figure 20. Displacement Thickness Distributions at M_∞ = .94

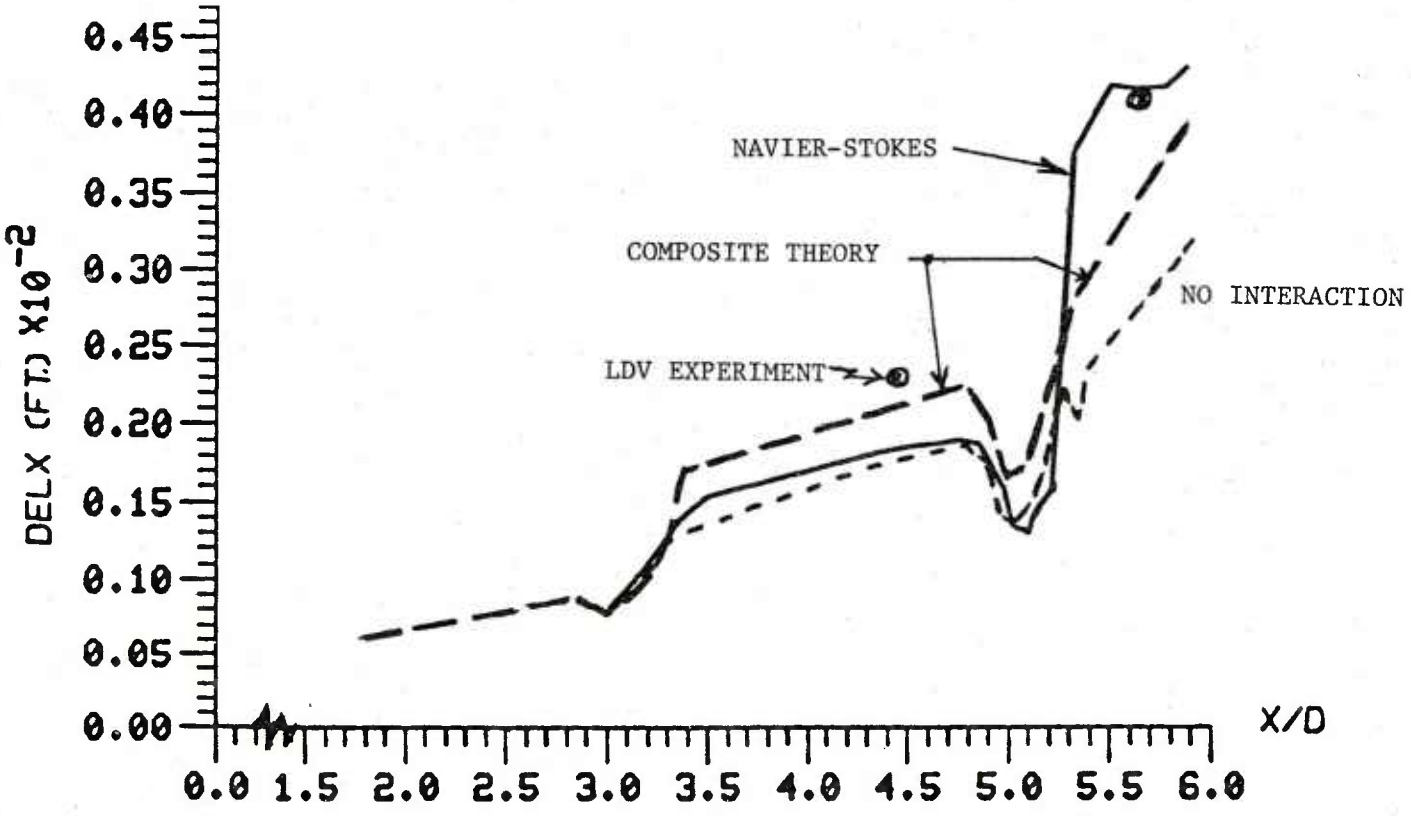

Figure 21. Comparison of Theoretical and Experimental Displacement Thickness Distributions at M_∞ = .908

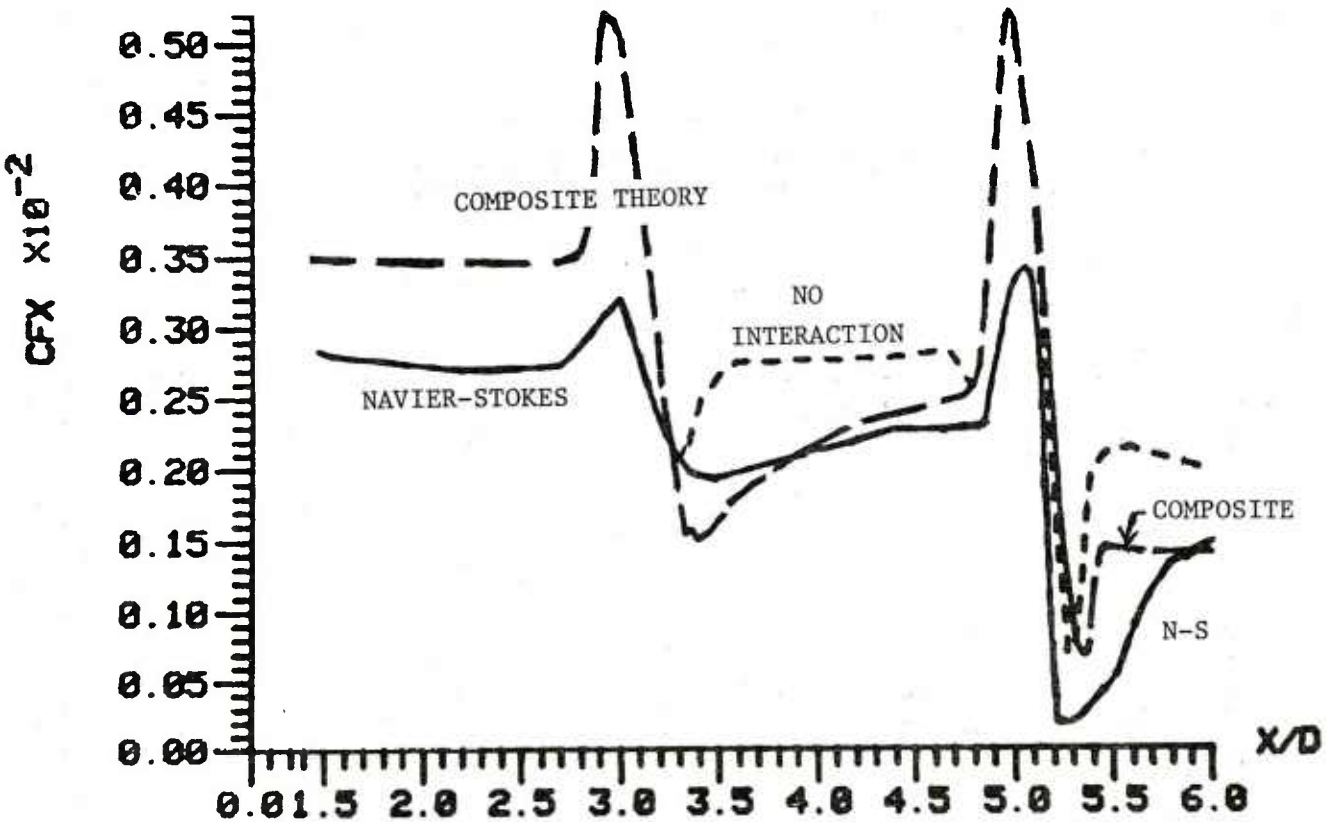

Figure 22. Composite Interaction Theory and Navier-Stokes Predictions for Skin Friction Distribution at M_∞ = .908

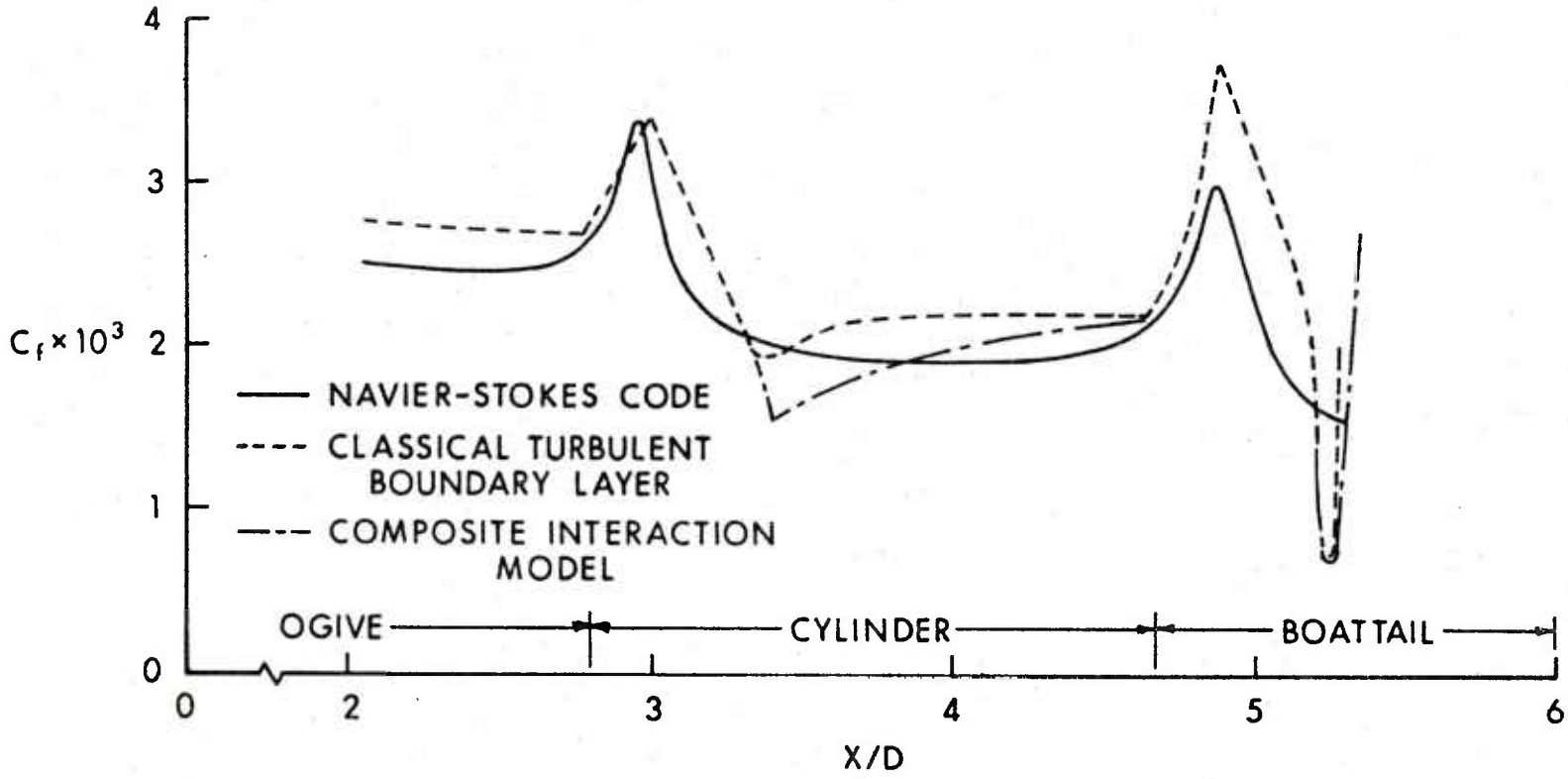

Figure 23. Theoretical Skin Friction Predictions at M_∞ = .94

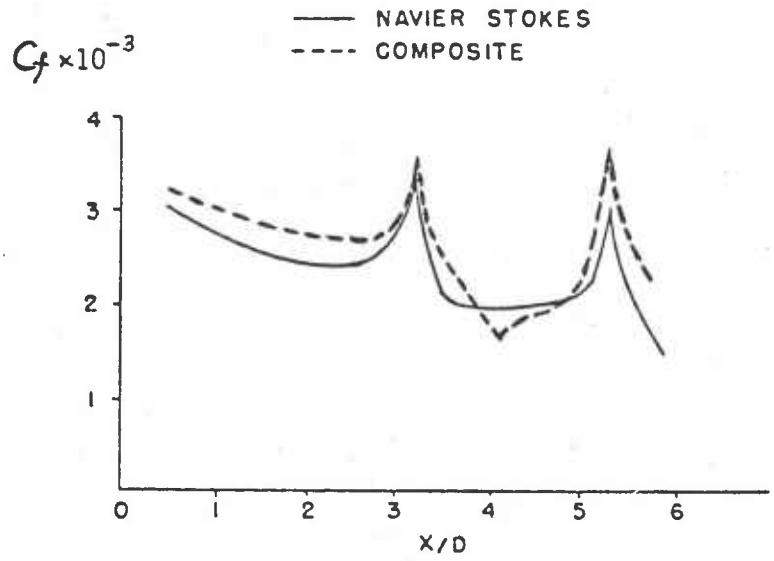

Figure 24. Theoretical Skin Friction Predictions at M_∞ = .97

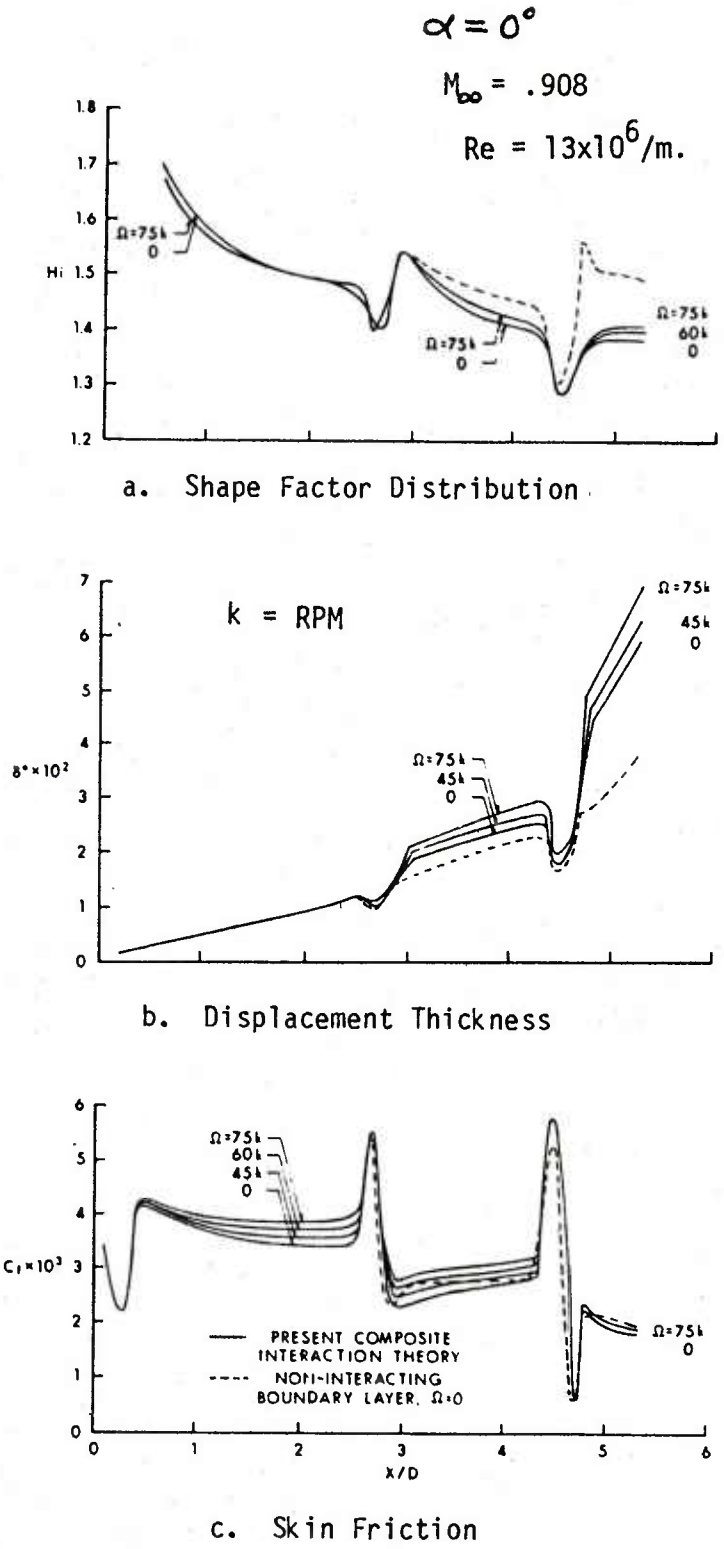

Figure 25. The Typical Influence of Spin on the Viscous-Inviscid Interaction Field Predicted by the Composite Theory

REFERENCES

1. Sturek, W. B., et al., "Computations of Magnus Effects for a Yawed, Spinning Body of Revolution," AIAA Journal, Vol. 16, No. 7, July 1978, pp. 687-692.

2. Rose, W. C., and Segniner, A., "Calculation of Transonic Flow Over Supercritical Airfoil Sections," AIAA Journal, Vol. 15, August 1978, pp. 514-519.

3. Sobieczky, M., and Stanewsky, E., "The Design of Transonic Airfoils Under Consideration of Shock Wave-Boundary Layer Interaction," 10 ICAS Congress Paper, October 1976 (see also E. Stanewsky and H. Zimmer, Zeit. fur Flugwissenschaften 23, Heft 7/8, 1975).

4. Wu, J. C., Moulden, T. H., and Uchiyama, N., "Aerodynamic Performance of Missile Configurations at Transonic Speeds Including the Effects of a Jet Plume," U.S. Army Missile Command Technical Report RD-76-23, Redstone Arsenal, Alabama, March 1976.

5. Reklis, R. P., Sturek, W. B., and Bailey, F. R., "Computation of Transonic Flow Past Projectiles at Angle of Attack," AIAA 11th Fluid and Plasma Dynamics Conference, AIAA Paper No. 78-1182, July 1978.

6. Inger, G. R., "Upstream Influence and Skin Friction in Non-Separating Shock Turbulent Boundary Layer Interactions," AIAA Paper No. 80-1411, Snowmass, Colorado, July 1980.

7. Ackeret, J., Feldman, F., and Rott, N., "Investigations of Compression Shocks and Boundary Layers in Gases Moving at High Speed," NACA TM-1113, January 1947.

8. Lighthill, M. J., "On Boundary Layers and Upstream Influence; II. Supersonic Flow Without Separation," Proc, Royal Soc. A 217, 1953, pp. 478-507.

9. Stratford, B. S., "The Prediction of Separation of the Turbulent Boundary Layer," Jour. Fluid Mech. 5, pp. 1-16, 1959.

10. Inger, G. R., and Mason, W. H., "Analytical Theory of Transonic Normal Shock-Boundary Layer Interaction," AIAA Paper 75-831, June 1975 (abbreviated version published in AIAA Journal 14, pp. 1266-72, September 1976).

11. Melnik, R. E., and Grossman, B., "Analysis of the Interaction of a Weak Normal Shock Wave with a Turbulent Boundary Layer," AIAA Paper 74-598, June 1974.

12. Adamson, T. C., and Feo, A., "Interaction Between a Shock Wave and a Turbulent Layer in Transonic Flow," SIAM Journal. Appl. Math 29, July 1975, pp. 121-144.

13. Gadd, G. E., "Interactions Between Wholly Laminar or Wholly Turbulent Boundary Layers and Shock Wave Strong Enough to Cause Separation," Jour. of the Aeronaut. Sci. 20, November 1953, pp. 729.

14. Honda, M., "A Theoretical Investigation of the Interaction Between Shock Waves and Boundary Layers," Jour. Aero/Space Sci. 25, November 1958, pp. 667-677.

15. Hankey, W., and Shang, J., "Numerical Solution of the Navier-Stokes Equations for Supersonic Turbulent Flow over a Compression Ramp," AIAA Paper 75-3, Pasadena, January 1975.

16. Green, J. E., "Interactions Between Shock Waves and Boundary Layers," in Progress of Aero. Sci., Vol. 11, Pergamon, N.Y., 1965, pp. 319.

17. Rose, W. C., Murphy, J. D., and Watson, E. E., "Interaction of an Oblique Shock Wave with a Turbulent Boundary Layer," AIAA Jour. 7, December 1969, pp. 2211-2221.

18. Hankey, W. L., and Holden, M. S., "Two-Dimensional Shock Wave-Boundary Layer Interactions in High Speed Flow," AGARDograph 203, June 1974.

19. Burggraf, O. R., "Asymptotic Theory of Separation and Attachment of a Laminar Boundary Layer on a Compression Ramp," in AGARD CP-168 - Flow Separation, 1975.

20. Werle, M., and Bertke, S. D., "Application of an Interacting Boundary Layer Model to the Supersonic Turbulent Separation Problem," University of Cincinnati Report AFL 76-4-21, August 1976.

21. Le Balleur, J. C., Peyret, R., and Vivand, H., "Numerical Studies in High Reynolds Number Aerodynamics," in Computers and Fluids, Vol. 8, Pergamon, 1980, pp. 1-30.

22. Ragab, S. A., and Nayfeh, A. H., "A Second Order Asymptotic Solution for Laminar Separation of Supersonic Flows Past Compression Ramps," AIAA 78-1132, 1978.

23. Murman, E. M., and Cole, J. D., "Calculation of Plane Steady Transonic Flow," AIAA Jour. 9, January 1971, pp. 114-121.

24. Yajnik, A., "Asymptotic Theory of Turbulent Wall Boundary Layer Flows," JFM 42, 1970, pp. 411-427.

25. Rose, W. C., and Childs, M. E., "Reynolds Shear Stress Measurements in a Compressible Boundary Layer within a Shock Wave-Induced Adverse Pressure Gradient," JFM 65, 1, 1974, pp. 177-188.

26. Cebeci, T., and Bradshaw, P., "Momentum Transfer in Boundary Layers, McGraw-Hill/Hemisphere," Wash., D.C., 1977, p. 365.

27. Burggraf, O. R., "The Compressibility Transformation and the Turbulent Boundary Layer Equation," Jour. of the Aerospace Sci. 29, 1962, pp. 434-439.

28. Van Driest, E. R., "Turbulent Boundary Layers in Compressible Fluid," Jour. of the Aeronaut. Sci. 18, March 1951, pp. 145-160.

29. Jobe, C. E., and Hankey, W. L., "Turbulent Boundary Layer Calculations in Adverse Pressure Gradient Flows," AIAA Paper 80-0136, Pasadena, January 1980.

30. Inger, G. R., "Shock Wave Penetration and Lateral Pressure Gradient Effects on Transonic Normal Shock-Turbulent Boundary Layer Interactions," AIAA Journal, Vol. 15, August 1977, pp. 1179-1200, plus Vol. 16, May 1978, p. 541.

31. Inger, G. R., "Application of a Shock-Boundary Layer Interaction Theory to Transonic Airfoil Analysis," AGARD CP-291, Colorado Springs, September 1980.

32. Walz, A., "Boundary Layers of Flow and Temperature," M.I.T. Press, Cambridge, Mass., 1969, pp. 113.

33. Nandanan, M., Stanewsky, E., and Inger, G. R., "A Computational Procedure for Transonic Airfoil Flow Including a Special Solution for Shock-Boundary Layer Interaction," AIAA Journal Vol. 19, Dec 1981, pp. 1540-46.

34. Dwyer, H. A., and Sanders, B. R., "Magnus Forces on Spinning Supersonic Cones. Part I. The Boundary Layer," AIAA Journal Vol. 14, April 1976, p. 498.

35. Nietubicz, C. J., Pulliam, T. H., and Steger, J. L., "Numerical Solution of the Azimuthal-Invariant Thin-Layer Navier-Stokes Equations," ARBRL-TR-02227, March 1980. AIAA Paper 79-0010, January 1979.

36. Stanewsky, E., Nanandan, N., and Inger, G. R., Proc. AGARD Symposium on "Computation of Viscous-Inviscid Interactions," AGARD CP-291, Colorado Springs, September 1980.

37. Danberg, J. E., Reklis, R. P., and Inger, G. R., "Pressure Distributions and Boundary Layer Profiles on a Yawed Projectile at Transonic Speeds," University of Delaware Technical Report No. 226, Department of Mechanical and Aerospace Engineering, April 1979 (see also AIAA Paper 79-1551, July 1979).

38. Nietubicz, C. J., unpublished wind tunnel data. To be published as a BRL Memorandum Report.

39. Delery, J.M., "Investigation of Strong Shock Turbulent Boundary Layer Interaction in 2-D Transonic Flows with Emphasis on Turbulence Phenomena," AIAA Paper 81-1245, Palo Alto, California, 1981.

LIST OF SYMBOLS

A	Van Driest-Cebeci wall turbulence damping parameter
C_f	skin friction coefficient, $2\tau_w/\rho_{e_o} U_{e_o}^2$
C_p	pressure coefficient, $2\ p'/\rho_{e_o} U_{e_o}^2$
H	boundary layer shape factor, δ^*/θ^*
H_i	incompressible shape factor
M	Mach number
p	static pressure
p'	interactive pressure perturbation, $p-p_1$
Δp	pressure jump across incident shock
Re_ℓ, Re_δ	Reynolds number based on length ℓ and boundary layer thickness, respectively
T	absolute temperature
$\mathcal{T}$	basic interactive wall-turbulence parameter (see Eq. 23)
u', v'	streamwise and normal interactive disturbance velocity components, respectively
U_o	undisturbed incoming boundary layer velocity in x-direction
x, y	streamwise and normal distance coordinates (origin at the inviscid shock intersection with the wall)
$y_{w_{eff}}$	effective wall shift seen by interactive inviscid flow (see Fig. 3)
β	$\sqrt{M_1^2-1}$
γ	specific heat ratio
δ	boundary layer thickness
δ^*	boundary layer displacement thickness
δ_{SL}	inner deck sublayer thickness
ε_T	kinematic turbulent eddy viscosity

ε_T'	interactive perturbation of turbulent eddy viscosity
η	y/δ_o
μ	molecular coefficient of viscosity
ν	μ/ρ
ω	viscosity-temperature dependence exponent, $\mu \sim T^{\omega}$
ρ	density
θ^*	boundary layer momentum thickness
τ	total shear stress
τ'	interactive perturbation of total shear stress

Subscripts

1	undisturbed inviscid values ahead of incident shock
e	conditions at the boundary layer edge
inc	incompressible value
inv	inviscid disturbance solution value
o	undisturbed incoming boundary layer properties

APPENDIX A

COMPOSITE LAW OF THE WALL-LAW OF THE WAKE TURBULENT VELOCITY PROFILE RELATIONSHIPS

APPENDIX A

COMPOSITE LAW OF THE WALL-LAW OF THE WAKE TURBULENT VELOCITY PROFILE RELATIONSHIPS

Because of its convenient analytical form, accurately blended representation of the combined Law of the Wall-Law of the Wake behavior and generality, we have adopted Walz's model[32] for the incoming turbulent boundary layer upstream of the interaction. For the low Mach number adiabatic wall conditions appropriate to transonic applications, it may be satisfactorily corrected for compressibility effects by the Eckert Reference Temperature method (which under these conditions is, in fact, comparable in accuracy to, but far simpler to implement than, the Van Driest compressibility transformation approach).

Let π be Coles (incompressible) Wake Function, $\eta \equiv y/\delta$ and denote for convenience $R \equiv .41\ Re\delta_o^*/[(1+\pi)(Tw/Te)^{1+\omega}]$ where $T_w/T_e \simeq 1 + .18\ Me_1^2$ and $\omega \simeq .76$ for a perfect gas; then the compressible form of Walz's composite profile may be written

$$\frac{U_o}{U_{oe}} = 1 + \frac{1}{.41}\sqrt{\frac{C_{fo}}{2}\left(\frac{Tw}{Te}\right)}\left[\left(\frac{R}{1+R}\right)\eta^2(1-\eta) + 2\pi\,\eta^2(3-2\eta) - 2\pi\right. \tag{A-1}$$

$$\left. + \ln\left(\frac{1+R\eta}{1+R}\right) - (2.15 + 1.235\,R\eta)e^{-.3R\eta}\right]$$

subject to the following condition linking π to C_{fo} and $Re\delta_o^*$ that derives from the $u \to ue$ matching condition at the boundary layer edge:

$$2\pi + 2.15 + \ln(1+R) = \frac{.41}{\sqrt{\frac{C_{fo}}{2}\left(\frac{Tw}{Te}\right)}} \tag{A-2}$$

Eqs. (A-1) and (A-2) have the following desireable properties: (a) for $\eta \geq .10$ or so, Uo is dominated by a Law of the Wake behavior which correctly satisfies both the outer limit conditions $Uo/Ue \to 1$ and $dU_o/dy \to 0$ as $\eta \to 1$; (b) on the other hand, for very small η values, Uo assumes a Law of the Wall-type behavior consisting of a logarithmic term that is exponentially damped out extremely close to the wall into a linear laminar sublayer profile $U_o/Ue \simeq R\eta$ as $\eta \to 0$; (c) Eq. (A-1) may be differentiated w.r.t. η to yield an analytical expression for dU_o/dy, which proves advantageous in solving the

middle and inner deck interaction problems (see text) where dM_o/dy must be known and vanish at the boundary layer edge.

The use of the incompressible form of (A-1) in the defining integral relations for δ_i^* and θ_i^* yields the following relationship that links the wake parameter to the resulting incompressible shape factor $H_{i1} = (\delta_i^*/\theta_i^*)_1$:

$$\frac{H_{i1} - 1}{H_{i1}} = \frac{2}{.41}\sqrt{\frac{T_w}{T_e}\frac{C_{fo}}{2}}\left(\frac{1+1.59\pi + .75\pi^2}{1 + \pi}\right) \qquad \text{(A-3)}$$

Eqs. (A-2) and (A-3) together with the defining relation for R enable a general and convenient parameterization of the profile (and hence the interaction that depends on it) in terms of the shock strength Me_1 the local displacement thickness Reynolds number $Re_{\delta o}^*$, and one additional physical parameter upstream of the shock. This parameter is taken to be the shape factor H_{i1} because it reflects the upstream history of the incoming boundary layer including possible pressure gradient and surface mass transfer effects. With this prescribed, the aforementioned three equations may be solved simultaneously for the attendant skin friction value C_{fo}, the value of R and, if desired, the π value appropriate to these flow conditions.

DISTRIBUTION LIST

No. of Copies	Organization
12	Administrator Defense Technical Info Center ATTN: DTIC-DDA Cameron Station Alexandria, VA 22314
1	Commander US Army Materiel Development and Readiness Command ATTN: DRCDMD-ST 5001 Eisenhower Avenue Alexandria, VA 22333
10	Commander US Army Armament Research and Development Command ATTN: DRDAR-TDC DRDAR-TSS DRDAR-LCA-F Mr. D. Mertz Mr. E. Falkowski Mr. A. Loeb Mr. R. Kline Mr. S. Kahn Mr. S. Wasserman Mr. H. Hudgins Dover, NJ 07801
1	Commander US Army Armament Materiel Readiness Command ATTN: DRSAR-LEP-L, Tech Lib Rock Island, IL 61299
1	Director US Army Armament Research and Development Command Benet Weapons Laboratory ATTN: DRDAR-LCB-TL Watervliet, NY 12189
1	Commander US Army Aviation Research and Development Command ATTN: DRDAV-E 4300 Goodfellow Blvd. St. Louis, MO 63120
1	Director US Army Air Mobility Research and Development Laboratory Ames Research Center Moffett Field, CA 94035
1	Commander US Army Communications Research and Development Command ATTN: DRDCO-PPA-SA Fort Monmouth, NJ 07703
1	Commander US Army Electronics Research and Development Command Technical Support Activity ATTN: DELSD-L Fort Monmouth, NJ 07703
2	Commander US Army Missile Command ATTN: DRSMI-R DRSMI-RDK Mr. R. Deep Redstone Arsenal, AL 35898
1	Commander US Army Missile Command ATTN: DRSMI-YDL Redstone Arsenal, AL 35898
1	Commander US Army Tank Automotive Research and Development Command ATTN: DRDTA-UL Warren, MI 48090
1	Director US Army TRADOC Systems Analysis Activity ATTN: ATAA-SL, Tech Lib White Sands Missile Range, NM 88002

DISTRIBUTION LIST

No. of Copies	Organization
1	Commander US Army Research Office P. O. Box 12211 ATTN: Dr. R. Singleton Research Triangle Park NC 27709
1	US Naval Academy ATTN: Mech Engineering Dept ATTN: Prof. J. Gillerlain Annapolis, Maryland 21402
1	Commander US Naval Air Systems Command ATTN: AIR-604 Washington, D. C. 20360
1	Commander ATTN: Dr. K. T. Yen, Code 3015 Naval Air Development Center Warminster, PA 18974
4	Commander David W. Taylor Naval Ship Research and Development Center ATTN: Dr. S. de los Santos Dr. Joanna Schot Dr. H. R. Chaplin Mr. Stanley Gottlieb Bethesda, Maryland 20084
5	Commander US Naval Surface Weapons Center ATTN: Dr. T. Clare, Code DK20 Mr. P. Daniels Mr. D. A. Jones III Mr. L. Mason Technical Library Dahlgren, VA 22448
4	Commander US Naval Surface Weapons Center ATTN: Code 312 Dr. C. Hsieh Dr. W. Yanta Dr. T. Zien Mr. R. Voisinet Silver Spring, MD 20910
1	Commander US Naval Weapons Center ATTN: Code 3431, Tech Lib China Lake, CA 93555
1	Chief Scientist USAF Arnold Engineering Development Center ATTN: Dr. B. Reese Arnold AF Station, TN 37389
3	Air Force Flight Dynamics Lab. ATTN: AFWL/FIM (Dr. W. Hankey) AFWAL/FIMG (Dr. A. Fiore) AFWAL/FS (Dr. G. Richey) Wright-Patterson Air Force Base Dayton, OH 45433
1	Library of Congress Science and Technology Division Washington, DC 20540
1	Director NASA Langley Research Center ATTN: NS-185, Tech Lib Langley Station Hampton, VA 23365
1	NASA ATTN: Library, MS 60-3 21000 Brookpark Road Cleveland, OH 44135
1	Director NASA Ames Research Center ATTN: MS-227-8 Dr. L. Schiff Moffett Field, CA 94035

DISTRIBUTION LIST

No. of Copies	Organization
1	Director of Research (Code RR) National Aeronautics and Space Administration 600 Independence Avenue, SW Washington, DC 20546
1	Nielsen Engineering & Research, Inc. ATTN: Dr. S. Stahara 510 Clyde Avenue Mountain View, CA 94043
3	Sandia Laboratories ATTN: Technical Staff, Dr. W.L. Oberkampf Aeroballistics Division 5631, G.R. Eisner H.R. Vaughn Albuquerque, NM 87115
1	President- Aeronautical Research Associates of Princeton ATTN: Dr. B. Quinn 50 Washington Road Princeton, NJ 08540
1	AVCO-Everett Research Laboratory ATTN: Technical Library 2385 Revere Beach Parkway Everett, MA 02149
1	Boeing Aerospace Company Boeing Military Airplane Development Organization ATTN: Dr. P. E. Rubbert P. O. Box 3707 Seattle, WA 98124
1	Boeing Aerospace Company ATTN: Dr. H. Yoshihara P. O. Box 3707 Mail Stop 41-18 Seattle, WA 98124
1	CALSPAN Corporation Advanced Technology Center ATTN: Dr. T. J. Falk P. O. Box 400 Buffalo, NY 14225
1	Douglas Aircraft Company, Inc. ATTN: Library 3855 Lakewood Boulevard Long Beach, CA 90801
1	General Dynamics-CONVAIR ATTN: Library & Info Services P. O. Box 1128 San Diego, CA 92112
1	General Electric Company Missile and Space Division ATTN: Mr. L. I. Chasen P. O. Box 8555 Philadelphia, PA 19101
1	Jet Propulsion Laboratory ATTN: Library 4800 Oak Grove Drive Pasadena, CA 91103
1	United Aircraft Corp Rsch Lab ATTN: Library Silver Lane East Hartford, CT 06108
1	Lockheed Missiles and Space CO. Technical Information Center 3251 Hanover Street Palo Alto, CA 94304
1	McDonnell Douglas Corporation ATTN: Engineering Library Department 218, Building 101 P. O. Box 516 St. Louis, MO 63166
1	Nielsen Engineering and Research, Inc. ATTN: Library 510 Clyde Avenue Mountain View, CA 94043
1	Northrop Corporation ATTN: Library Aircraft Division 3901 West Broadway Hawthorne, CA 90250

DISTRIBUTION LIST

No. of Copies	Organization
1	Rockwell International Science Center ATTN: Library 1049 Camino Dos Rios P. O. Box 1085 Thousand Oaks, CA 91360
1	LTV Aerospace Corporation ATTN: Tech Library 2-51131 P. O. Box 5907 Dallas, TX 75222
1	TRW Systems Group, Inc. ATTN: Library One Space Park Redondo Beach, CA 90278
1	California Institute of Technology Department of Aeronautics ATTN: Prof. H. Liepmann Pasadena, CA 91102
1	Massachusetts Institute of Technology ATTN: Tech Library 77 Massachusetts Avenue Cambridge, MA 02139
1	Ohio State University Department of Aeronautical and Astronautical Engineering ATTN: Prof. O. Burggraf 1314 Kinnear Road Columbus, OH 43212
1	Princeton University Gas Dynamics Laboratory Department of Aerospace and Mechanical Sciences ATTN: Prof. S. Bogdonoff Princeton, NJ 08540
1	San Diego State University College of Engineering ATTN: Dr. K. C. Wang San Diego, CA 92182
1	Stanford University Department of Aeronautics and Astronautics ATTN: Prof. J. Steger Stanford, CA 94035
1	University of California Mechanics and Structures Dept. School of Engineering and Applied Science ATTN: Prof. J. D. Cole Los Angeles, CA 90024
1	University of California, Davis Department of Mechanical Engineering ATTN: Prof. H.A. Dwyer Davis, CA 95616
2	University of Cincinnati Department of Aerospace Engineering & Applied Mechanics ATTN: Prof. R. T. Davis Prof. S. G. Rubin Cincinnati, OH 45221
1	University of Colorado Department of Aerospace Engineering Sciences ATTN: Prof. G. Inger Boulder, CO 80309
1	University of Delaware Mechanical and Aerospace Engineering Department ATTN: Dr. J. E. Danberg Newark, DE 19711
1	University of Florida ATTN: Dr. J.E. Milton P.O. Box 1918 Eglin AFB, FL 32542

DISTRIBUTION LIST

No. of Copies	Organization
1	University of Maryland College of Engineering ATTN: Dr. J. D. Anderson, Jr. Chairman, Department of Aerospace Engineering College Park, MD 20742
1	University of Notre Dame Department of Aerospace/ Mechanical Engineering ATTN: Prof. T. J. Mueller Notre Dame, IN 46556

Aberdeen Proving Ground

Dir, USAMSAA
ATTN: DRXSY-D
DRXSY-MP, H. Cohen

Cdr, USATECOM
ATTN: DRSTE-TO-F

Dir, USACSL, Bldg. E3516, EA
ATTN: DRDAR-CLB-PA